Advances in Colloid and Interface Science 154 (2010) 91–103

Contents lists available at ScienceDirect

Advances in Colloid and Interface Science

journal homepage: www.elsevier.com/locate/cis

Capillary forces between particles at a liquid interface: General theoretical approach and interactions between capillary multipoles

Krassimir D. Danov, Peter A. Kralchevsky *

Department of Chemical Engineering, Faculty of Chemistry, University of Sofia, 1164 Sofia, Bulgaria

ARTICLE INFO

Available online 6 February 2010

Keywords:
Particles at liquid interfaces
Lateral capillary interactions
Forces between capillary multipoles

ABSTRACT

The liquid interface around an adsorbed colloidal particle can be undulated because of roughness or heterogeneity of the particle surface, or due to the fact that the particle has non-spherical (e.g. ellipsoidal or polyhedral) shape. In such case, the meniscus around the particle can be expanded in Fourier series, which is equivalent to a superposition of capillary multipoles, viz. capillary charges, dipoles, quadrupoles, etc. The capillary multipoles attract a growing interest because their interactions have been found to influence the self-assembly of particles at liquid interfaces, as well as the interfacial rheology and the properties of particle-stabilized emulsions and foams. As a rule, the interfacial deformation in the middle between two adsorbed colloidal particles is small. This fact is utilized for derivation of accurate asymptotic expressions for calculating the capillary forces by integration in the midplane, where the Young–Laplace equation can be linearized and the superposition approximation can be applied. Thus, we derived a general integral expression for the capillary force, which was further applied to obtain convenient asymptotic formulas for the force and energy of interaction between capillary multipoles of arbitrary orders. The new analytical expressions have a wider range of validity in comparison with the previously published ones. They are applicable not only for interparticle distances that are much smaller than the capillary length, but also for distances that are comparable or greater than the capillary length.

Contents

1. Introduction

The attachment of a solid particle to the boundary between two fluid phases can be accompanied by deformation of the liquid interface near the particle. The overlapping of deformations around two adsorbed particles gives rise to capillary interaction between them. In most cases, this interaction is attractive and engenders particle aggregation and ordering. The lateral capillary forces play an essential role in many physicochemical processes and the two-dimensional structures produced under their action have found numerous applications; see e.g. Refs. [1–8].

There are several different physical reasons for distortion of the liquid interface by an adsorbed particle. First, gravity-induced

* Corresponding author.
E-mail address: pk@lcpe.uni-sofia.bg (P.A. Kralchevsky).

0001-8686/$ – see front matter © 2010 Elsevier B.V. All rights reserved.
doi:10.1016/j.cis.2010.01.010

interfacial deformations (and capillary forces) appear due to the particle weight and the buoyancy force, which push the particle downwards or upwards depending on its relative density [9–13]. Second, the wettability of the particle surface by the liquid phase determines the position of the three-phase contact line on the particle surface thus creating menisci around particles confined in thick [14–20] and thin [21,22] liquid films. (In this context, the film is 'thin' if its thickness is much smaller than the particle diameter.) Third, the electric field of charged particles induces deformations in the liquid interface and electrodipping force [23–30].

For typical densities of colloidal particles, the weight of μm-sized and sub-μm-sized adsorbed particles is insufficient to deform the fluid interface and to bring about gravity-induced capillary interaction between the particles [11]. In this case, interfacial deformations can appear if the contact line at the particle surface has undulated or irregular shape. This may happen if the particle surface is rough, angular or heterogeneous. In such cases, the contact line sticks to edges or to boundaries between domains on the heterogeneous surface. The undulated contact line induces undulations in the surrounding fluid interface [31–34]. The theory predicts that an undulation of amplitude 50 nm in the contact line around a spherical particle leads to a long-range interaction energy that can exceed 10^4 kT in magnitude (k — Boltzmann constant; T — temperature) [32,33], which is a striking result. Such small deformations are difficult for detection, but their presence might be inferred from studies on the interaction between μm-sized particles in adsorption monolayers [35–37] and from the rheological behavior of particulate monolayers [38,39]. A numerical technique to calculate the free energy associated with the adsorption of a colloidal particle of complex shape at a liquid interface was recently proposed [40].

Let us consider two adsorbed spherical particles with undulated contact lines, which induce undulations in the surrounding liquid interface. The left- and right-hand-side particles will be denoted as "particle A" and "particle B", respectively (Fig. 1). The interfacial shape around each particle in isolation, $z=\zeta_Y(x,y)$, $Y=A$, B, obeys the linearized Young–Laplace equation [34]:

$$\frac{1}{\rho_Y}\frac{\partial}{\partial\rho_Y}\left(\rho_Y\frac{\partial\zeta_Y}{\partial\rho_Y}\right)+\frac{1}{\rho_Y^2}\frac{\partial^2\zeta_Y}{\partial\phi_Y^2}=q^2\zeta_Y \quad (Y=A,B) \tag{1.1}$$

where small meniscus slope is presumed; (ρ_A,ϕ_A) and (ρ_B,ϕ_B) are polar coordinates associated, respectively, with the left- and right-hand-side particle (Fig. 1); q is the inverse capillary length:

$$q^2\equiv\frac{\Delta\rho g}{\gamma}. \tag{1.2}$$

$\Delta\rho$ is the difference between the mass densities of the lower and upper fluid phases; γ is the tension of the interface between them; g is the acceleration due to gravity. The solution of Eq. (1.1) can be expressed as a Fourier multipole expansion [33,34]:

$$\zeta_Y=\sum_{m=0}^{\infty}\zeta_{Y,m}, \quad Y=A,B \tag{1.3}$$

$$\zeta_{Y,m}=h_{Y,m}\frac{K_m(q\rho_Y)}{K_m(qr_Y)}\cos\left[m\left(\phi_Y-\phi_{Y,m}\right)\right] \tag{1.4}$$

where K_m is the modified Bessel function of second kind and order m; $h_{Y,m}$ and $\phi_{Y,m}$ are the amplitude and phase shift for the m-th mode of undulation of the particle contact line; r_Y is the radius of its vertical projection on the xy-plane (Fig. 1). The terms with $m=0$, 1, 2, 3,..., respectively, play the role of capillary "charges", "dipoles", "quadrupoles", "hexapoles", etc. [3,32–34]. For a freely floating particle, the dipolar term with $m=1$ disappears because it is annihilated by a spontaneous rotation of the particle around a horizontal axis (unless the particle is fixed to a holder) [32]. For such a particle, the "capillary charge" term (with $m=0$) accounts for the interfacial distortion due to gravity, which is negligible for particles of micrometer and sub-micrometer size. Therefore, for small freely floating particles the leading term in interfacial deformation is the quadrupolar one, with $m=2$ [32,33].

As an illustration, in Fig. 2 we present contour-plot diagrams calculated from Eq. (1.4) that represent the meniscus shape around a capillary hexapole ($m=3$, Fig. 2a) and a capillary octupole ($m=4$, Fig. 2b). In these diagrams, the horizontal distances are scaled with r_Y. The vertical distance, ζ_Y, scaled with the amplitude of the undulations at the contact line, $h_{Y,m}$, is presented by colors in analogy with the geographic isoline maps.

Undulated contact lines are formed even on smooth surfaces if the shape of the particle is not spherical. Loudet et al. [41–43], investigated experimentally and theoretically the capillary forces between adsorbed ellipsoidal particles and found that they behave as capillary quadrupoles. These authors noted that from a purely geometrical viewpoint, the condition of a constant contact angle cannot be met for anisotropic particles if the interface remains flat, which explains the reason for the quadrupolar interfacial deformation. Lateral capillary forces between ellipsoidal and anisotropic particles have been investigated also by van Nierop et al. [44], Lehle et al. [45], and Stebe et al. [46,47].

The theoretical investigations of interactions between capillary quadrupoles and hexapoles indicate that this interaction is non-monotonic: attractive at long distances, but repulsive at short distances [33,34]. Expressions for the rheological properties (surface dilatational and shear elasticity and yield stress) of Langmuir monolayers from angular particles have been derived [31,33,34]. Mesoscale capillary multipoles have been experimentally realized by Bowden et al. [48–50] by appropriate hydrophobization or hydrophilization of the sides of small floating plates. Interactions between capillary quadrupoles have been observed between floating particles, which have the shape of curved disks [51] ellipsoids [41–43] and other anisotropic particles [46,47]. For multipoles, the sign and magnitude of the capillary force depend on the particle mutual orientation (on the angles $\phi_{A,m}$ and $\phi_{B,m}$). For that reason, particles–quadrupoles ($m=2$) will tend to assemble in a square lattice [51], whereas particles–hexapoles ($m=3$) will preferably form a hexagonal lattice, with or without voids [49,50]. Another possibility is the particles to form simple linear (chain) aggregates [3,32,51] or capillary arrows [43]. Quadrupolar interfacial deformation and the corresponding force can be produced also by the electric field of particles with anisotropic distribution of electric charges on their surfaces [52,53].

The effect of the interactions between capillary multipoles has been invoked to explain the properties of particulate monolayers at liquid interfaces [35–37,54–61], including powder particles [56],

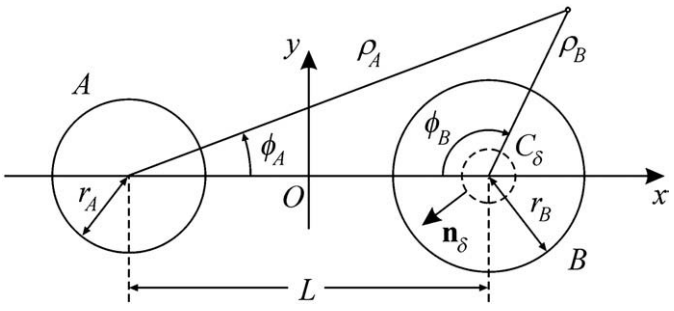

Fig. 1. Polar coordinates (ρ_A,ϕ_A) and (ρ_B,ϕ_B) in the xy-plane connected with the particles A and B. The projections of the contact lines on the particle surfaces are presented by two solid circles of radii r_A and r_B. The dashed circle C_δ, with outer unit normal $\mathbf{n}_\delta$, is an auxiliary contour of radius r_δ used for the derivation of the expression for the capillary force (see the text).

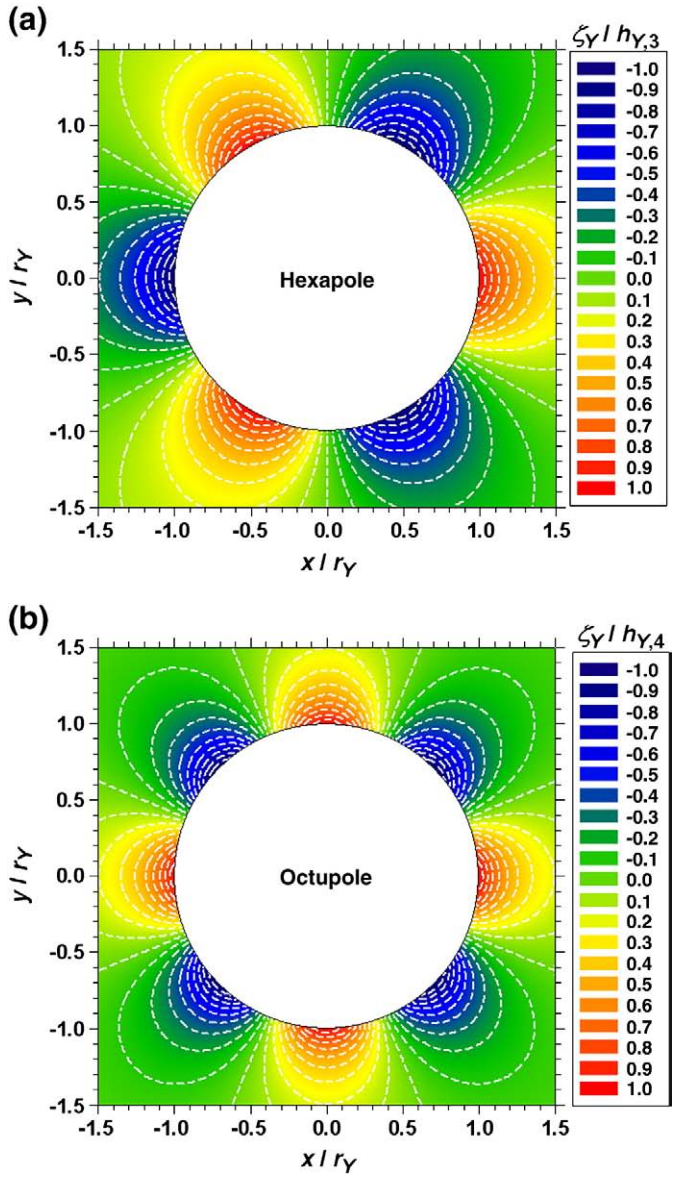

Fig. 2. Contour-plot diagram of the meniscus shape $z=\zeta_Y(x,y)$ (a) around a capillary hexapole ($m=3$) and (b) around a capillary octupole ($m=4$), calculated from Eq. (1.4). The x and y coordinates are scaled with r_Y, whereas the vertical coordinate ζ_Y is scaled with the amplitude of the undulations at the contact line, $h_{Y,m}$; see the text for the notations.

capillary retention of colloids in porous media [57] and ordering of nanowire-like objects [62]. These strong anisotropic capillary interactions lead to jamming of particle monolayers [63], and increasing of the elasticity and viscosity of adsorption layers, emulsions and foams [38,39,64–67]. In particular, Madivala et al. [66,67] experimentally established that monolayers of ellipsoids exhibit a substantial surface shear modulus even at low surface coverage and can be used to create more elastic monolayers compared to aggregate networks of spheres of the same size and surface properties. The experimental magnitude of the shear modulus, 10–100 mN/m, is in agreement with the theoretical predictions [33,34]. Another interesting experimental finding is that Pickering emulsions with adsorbed ellipsoidal particles become stable when the particle aspect ratio becomes greater than a certain critical value [67]. One possible explanation of this result can be related to the increase of interparticle capillary attraction with the rise of aspect ratio, which would help for the formation of dense adsorption layers that protect the emulsion drops against coalescence.

Using the asymptotic behavior of the modified Bessel function $K_m(x)$ at $x \ll 1$ [68,69]

$$K_m(x) \approx \frac{(m-1)!}{2}\left(\frac{2}{x}\right)^m \quad (x \ll 1, m = 1, 2, \ldots) \tag{1.5}$$

we can simplify Eq. (1.4) [32,33]:

$$\zeta_Y = h_{Y,m}\left(\frac{r_Y}{\rho_Y}\right)^m \cos\left[m\left(\phi_Y - \phi_{Y,m}\right)\right] \tag{1.6}$$

($Y=A, B$; $m=1, 2, \ldots$), where the assumptions $qr_Y \ll 1$ and $q\rho_Y \ll 1$ have been used. Under the same simplifying assumptions, it was established that the energy of interaction between the particles A and B, that behave as capillary multipoles of orders m and n, respectively, is given by the expression [34]:

$$\Delta W \approx -\frac{2\pi(m+n-1)!}{(m-1)!(n-1)!}\gamma h_{A,m}h_{B,n}\frac{r_A^m r_B^n}{L^{m+n}}\cos\left(m\phi_{A,m} - n\phi_{B,n}\right) \text{ for } qL \ll 1 \tag{1.7}$$

where L is the distance between the particles (Fig. 1). One can check that Eq. (1.7) is identical to the respective result in Ref. [34], having in mind that the phase-shift angles in Ref. [34] are defined as $\pi - \phi_{Y,m}$, where $\phi_{Y,m}$ is the phase-shift angle in the present article. (Our present definition leads to the disappearance of the factor $(-1)^{m+n}$ from the expressions for the energy and force of interaction.) Note that Eq. (1.7) can be obtained by integrating the expression for the respective capillary force; see Eq. (3.28) below. Eq. (1.7) shows that $\Delta W \propto 1/L^{m+n}$, i.e. at larger distance L the interaction energy ΔW decays faster for multipoles of greater net order $m+n$.

Eq. (1.7) shows explicitly the dependence of the energy of capillary interaction on the particle mutual orientation through the multiplier $\cos(m\phi_{A,m} - n\phi_{B,n})$. The energetically most favorable state is that for which the cosine is equal to $+1$, whereas the most disadvantageous state is that for which the cosine equals -1. Fig. 3 shows contour-plot diagrams of the meniscus shapes for the most advantageous ($\phi_{A,2} = \phi_{B,2}$) and disadvantageous ($\phi_{A,2} - \phi_{B,2} = \pi/2$) orientations for two capillary quadrupoles. In the calculations (see Appendix A for details), we have used the analytical solution of the problem in bipolar coordinates in Ref. [34], which allows one to exactly satisfy the boundary conditions at the contact lines on the surfaces of the two particles. This asymptotic solution is applicable for calculating the meniscus shape in the vicinity of small particles, where $q\rho_Y \ll 1$.

Eq. (1.7) is applicable for relatively short distances ($qL \ll 1$) between small particles ($qr_Y \ll 1$). However, Eq. (1.7) is at the limit of its applicability or inapplicable for mesoscale particles of diameter ≥ 500 μm like those studied in Refs. [48–50]. Moreover, the attraction between small particles leads to the formation of two-dimensional aggregates [70–73]. Although the gravitational deformation in the liquid interface might be negligible for an isolated particle, it can become significant for an aggregate, and then the use of expressions in terms of the K_m-functions is obligatory.

Our goal in the present article is to obtain a generalized form of Eq. (1.7), which is valid for both short and long distances between capillary multipoles of various orders $m,n = 0, 1, 2, 3, \ldots$. For this goal, we have to work in terms of the functions $K_m(q\rho_Y)$, see Eq. (1.4). The results will contain as special cases the short-range asymptotics like Eqs. (1.5)–(1.7). In Section 2, we derive general integral expressions for the lateral capillary forces. In Section 3, this approach is applied to obtain analytical formulas for calculating the forces between two capillary multipoles of arbitrary order.

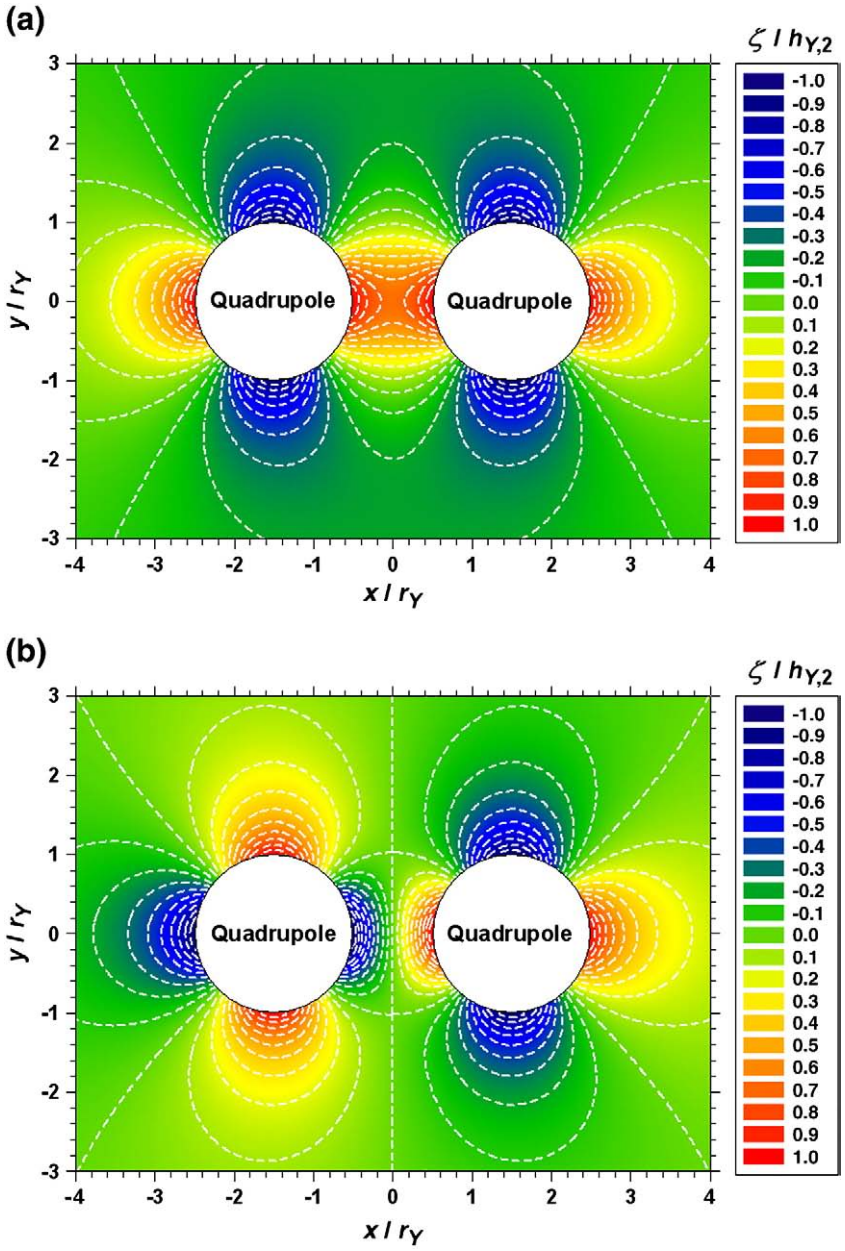

Fig. 3. Contour-plot diagram of the meniscus shape $z=\zeta(x,y)$ around two similar capillary quadrupoles ($m=n=2$) with $r_Y=r_A=r_B$, separated at a center-to-center distance $L=3r_Y$; see Appendix A for the procedure of calculations. (a) The most advantageous ($\phi_{A,2}=\phi_{B,2}$) and (b) the most disadvantageous ($\phi_{A,2}-\phi_{B,2}=\pi/2$) mutual orientation of the two quadrupoles with respect to their interaction energy; see Eq. (1.7). The scaling of x, y and ζ is the same as in Fig. 2.

2. General expressions for the lateral capillary force

2.1. Calculation of the capillary force by integration over the midplane

Our first goal is to derive a general expression for the lateral capillary force between two particles, which will be further applied to quantify the interaction between floating particles that behave as capillary multipoles of different orders. For this goal, let us consider two spherical particles separated at a center-to-center distance L. The liquid interface is assumed to be planar in the absence of adsorbed particles. The xy-plane of the coordinate system is chosen to coincide with the non-disturbed liquid interface. The x-axis passes through the vertical axes of the two particles, and the yz-plane is located in the middle between the two particles. The lower and upper fluid phases are denoted, respectively, as "phase I" and "phase II" (Fig. 4). Each separate particle creates deformation in the surrounding liquid interface. The meniscus shape around the particles is given by the equation $z=\zeta(x,y)$.

At hydrostatic equilibrium, the divergence of the pressure tensor in each of the two neighboring fluid phases is equal to zero [74]:

$$\nabla\cdot\mathbf{P}_{\mathrm{I}}=\mathbf{0} \quad \text{and} \quad \nabla\cdot\mathbf{P}_{\mathrm{II}}=\mathbf{0} \tag{2.1}$$

where ∇ denotes the del operator; $\mathbf{P}_{\mathrm{I}}$ and $\mathbf{P}_{\mathrm{II}}$ are the pressure tensors in the phases "I" and "II". (Note that by definition, the pressure tensor is $\mathbf{P}=-\hat{\mathbf{T}}$, where $\hat{\mathbf{T}}$ is the stress tensor.) In addition, at equilibrium the shape of the liquid interface obeys the Laplace equation of capillarity:

$$2H\gamma=\mathbf{n}_{\mathrm{s}}\cdot(\mathbf{P}_{\mathrm{II}}-\mathbf{P}_{\mathrm{I}})\cdot\mathbf{n}_{\mathrm{s}} \quad \text{at} \quad z=\zeta \tag{2.2}$$

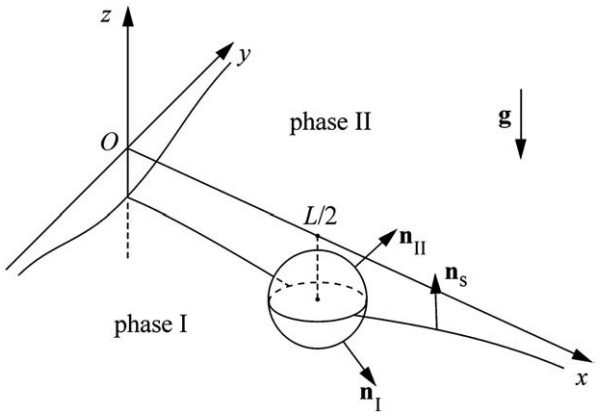

Fig. 4. Sketch of a particle that is attached to the interface between phases "I" and "II". The vertical *yz*-plane represents the midplane between two particles (like those in Fig. 1). The horizontal *xy*-plane coincides with the unperturbed liquid interface far from the particles. The *x*-axis is directed as in Fig. 1.; $\mathbf{n}_I$, $\mathbf{n}_{II}$ and $\mathbf{n}_s$ are unit vector fields normal to the interfaces particle/phase I; particle/phase II, and to the liquid interface, respectively.

where H is the mean curvature of the liquid surface $z=\zeta(x,y)$; $\mathbf{n}_s$ is the running unit normal to this surface directed toward phase II, and γ is the interfacial tension.

Let us consider the right-hand-side particle shown in Fig. 4 (for the left-hand-side particle the consideration is analogous). The force acting on this particle can be expressed in the form [16]

$$\mathbf{F} = \mathbf{F}^{(p)} + \mathbf{F}^{(\gamma)} \tag{2.3}$$

$\mathbf{F}^{(p)}$ is the integral of pressure tensor over the particle surface and $\mathbf{F}^{(\gamma)}$ is the integral of the interfacial tension, considered as a vector, over the contact line on particle surface, C:

$$\mathbf{F}^{(p)} = -\int_{S_I} dS\mathbf{n}_I\cdot\mathbf{P}_I - \int_{S_{II}} dS\mathbf{n}_{II}\cdot\mathbf{P}_{II}\,, \qquad \mathbf{F}^{(\gamma)} = \int_C dl\mathbf{m}\gamma \tag{2.4}$$

where S_I and S_{II} are the portions of the particle surface that contact with phases I and II, respectively; $\mathbf{n}_I$ and $\mathbf{n}_{II}$ are outer unit normal fields with respect to the particle (Fig. 4); dl is the scalar linear element of the contact line C; $\mathbf{m}$ is the outward pointing unit normal field having the direction of the surface tension at the contact line, i.e. normal to C and tangential to the liquid interface.

To calculate $\mathbf{F}^{(\gamma)}$, we will use the fact that the Laplace equation, Eq. (2.2), is the normal projection (along $\mathbf{n}_s$) of a more general equation; see e.g. Ref. [1]:

$$\nabla_s\cdot(\gamma\mathbf{U}_s) = \mathbf{n}_s\cdot(\mathbf{P}_{II}-\mathbf{P}_I) \quad \text{at} \quad z=\zeta \tag{2.5}$$

where ∇_s and $\mathbf{U}_s$ are the del operator and the unit tensor of the surface $z=\zeta(x,y)$. Following the approach proposed in Ref. [75], we consider a rectangle EFMN situated in the *xy*-plane as shown in Fig. 5. Next, we integrate Eq. (2.5) over the surface S_{EFMN}, which represents the vertical projection of the rectangle EFMN on the interface $z=\zeta(x,y)$:

$$\int_{S_{EFMN}} dS\mathbf{n}_s\cdot(\mathbf{P}_{II}-\mathbf{P}_I) = \int_{S_{EFMN}} dS\nabla_s\cdot(\gamma\mathbf{U}_s) = \int_{C_{EFMN}} dl\mathbf{m}\gamma - \mathbf{F}^{(\gamma)} \tag{2.6}$$

where the contour C_{EFMN} is the periphery of S_{EFMN} and we have used the two-dimensional divergence theorem [1,76]. Using the fact that the meniscus $z=\zeta(x,y)$ decays at infinity, we assume that the points

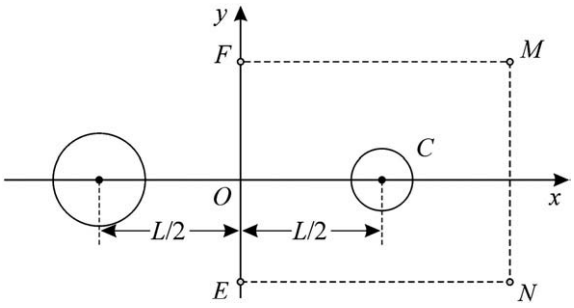

Fig. 5. Integration domains for calculating the interaction force between two particles (details in the text). The projections of the contact lines on the particle surfaces are presented by two circles, but they could be arbitrary closed contours. The force of interaction between the two particles is directed along the *x*-axis.

E, F, M and N are located far from the particle, and then the *x*-projection of Eq. (2.6) acquires the form:

$$F_x^{(\gamma)} \equiv \mathbf{e}_x\cdot\mathbf{F}^{(\gamma)} = \int_{C_{EF}\cup C_{MN}} dl(\mathbf{e}_x\cdot\mathbf{m})\gamma - \int_{S_{EFMN}} dS\mathbf{n}_s\cdot(\mathbf{P}_{II}-\mathbf{P}_I)\cdot\mathbf{e}_x \tag{2.7}$$

Next, we consider a right prism built on the rectangle EFMN with lower and upper bases situated deeply inside the phases I and II. In view of Eq. (2.1), we have:

$$0 = \int_{V^I} dV\nabla\cdot\mathbf{P}_I = \oint_{\partial V^I} d\mathbf{S}\cdot\mathbf{P}_I \tag{2.8}$$

where V^I is the portion of the aforementioned vertical prism that is located in the phase I, and ∂V^I is the surface of V^I; d$\mathbf{S}$ is the respective outward pointing vectorial surface element. In view of the symmetry of the system, the *x*-projection of Eq. (2.8) can be presented in the form:

$$0 = \mathbf{e}_x\cdot\left[\int_{S_{EFMN}} dS\mathbf{n}_s\cdot\mathbf{P}_I + \int_{S_{EF}^{(I)}} d\mathbf{S}\cdot\mathbf{P}_I + \int_{S_{MN}^{(I)}} d\mathbf{S}\cdot\mathbf{P}_I - \int_{S_I} dS\mathbf{n}_I\cdot\mathbf{P}_I\right] \tag{2.9}$$

Here, $S_{EF}^{(I)}$ and $S_{MN}^{(I)}$ are the portions of the vertical planes passing through the segments EF and MN, which are in contact with the phase I; S_I is the same in Eq. (2.4). In a similar way, we derive a counterpart of Eq. (2.9) for the phase II:

$$0 = \mathbf{e}_x\cdot\left[-\int_{S_{EFMN}} dS\mathbf{n}_s\cdot\mathbf{P}_{II} + \int_{S_{EF}^{(II)}} d\mathbf{S}\cdot\mathbf{P}_{II} + \int_{S_{MN}^{(II)}} d\mathbf{S}\cdot\mathbf{P}_{II} - \int_{S_{II}} dS\mathbf{n}_{II}\cdot\mathbf{P}_{II}\right] \tag{2.10}$$

In view of Eq. (2.4), we sum Eqs. (2.9) and (2.10):

$$F_x^{(p)} \equiv \mathbf{e}_x\cdot\mathbf{F}^{(p)} = \mathbf{e}_x\cdot\left[\int_{S_{EFMN}} d\mathbf{S}\cdot(\mathbf{P}_{II}-\mathbf{P}_I) - \int_{S_{EF}} d\mathbf{S}\cdot\mathbf{P} - \int_{S_{MN}} d\mathbf{S}\cdot\mathbf{P}\right] \tag{2.11}$$

where $S_{EF}=S_{EF}^{(I)}\cup S_{EF}^{(II)}$ and $S_{MN}=S_{MN}^{(I)}\cup S_{MN}^{(II)}$ are stripes of vertical planes that are based on the segments EF and MN;

$$\mathbf{P}\equiv\mathbf{P}_I \quad \text{for} \quad z<\zeta, \quad \text{and} \quad \mathbf{P}\equiv\mathbf{P}_{II} \quad \text{for} \quad z>\zeta \tag{2.12}$$

Next, we sum up Eqs. (2.7) and (2.11); the integrals over S_{EFMN} cancel each other, and we obtain the following expression for the total force acting on the right-hand side particle (see Fig. 4):

$$F_x \equiv F_x^{(\gamma)} + F_x^{(p)} = \int_{C_{EF}\cup C_{MN}} dl(\mathbf{e}_x\cdot\mathbf{m})\gamma - \int_{S_{EF}\cup S_{MN}} d\mathbf{S}\cdot\mathbf{P}\cdot\mathbf{e}_x \tag{2.13}$$

Let us denote the first and the second integral in the right-hand side of Eq. (2.13) by $F_x^{(C)}$ and $F_x^{(S)}$, respectively. Because the segments EF and MN

are perpendicular to the x-axis, and the points E, F, M and N (by definition) are located far away from the particle, we have:

$$F_x^{(C)} \equiv \int\limits_{C_{EF}\cup C_{MN}} dl(\mathbf{e}_x\cdot\mathbf{m})\gamma = \gamma\int\limits_{-\infty}^{\infty} dy\left\{1-\left[\left(1+\zeta_y^2\right)/\left(1+\zeta_x^2\right)\right]^{1/2}\right\}\Bigg|_{x=0} \tag{2.14}$$

where $\zeta_x \equiv \partial\zeta/\partial x$, $\zeta_y \equiv \partial\zeta/\partial y$ and $\gamma = \text{const}$. Likewise, we obtain:

$$F_x^{(S)} \equiv -\int\limits_{S_{EF}\cup S_{MN}} d\mathbf{S}\cdot\mathbf{P}\cdot\mathbf{e}_x = \int\limits_{-\infty}^{\infty}\int\limits_{-\infty}^{\infty} dydz\mathbf{e}_x\cdot(\mathbf{P}|_{x=0}-\mathbf{P}|_{x\to\infty})\cdot\mathbf{e}_x. \tag{2.15}$$

Having in mind the definition of $\mathbf{P}$ by Eq. (2.12), we can represent the above expression in the form:

$$F_x^{(S)} = \int\limits_{-\infty}^{\infty} dy\left[\int\limits_{-\infty}^{\zeta} dz\ \mathbf{e}_x\cdot\mathbf{P}_{I,0}\cdot\mathbf{e}_x - \int\limits_{-\infty}^{0} dz\mathbf{e}_x\cdot\mathbf{P}_{I,\infty}\cdot\mathbf{e}_x\right] + \int\limits_{-\infty}^{\infty} dy\left[\int\limits_{\zeta}^{\infty} dz\mathbf{e}_x\cdot\mathbf{P}_{II,0}\cdot\mathbf{e}_x - \int\limits_{0}^{\infty} dz\mathbf{e}_x\cdot\mathbf{P}_{II,\infty}\cdot\mathbf{e}_x\right] \tag{2.16}$$

where the subscripts "0" and "∞" denote the values of the respective quantity at $x = 0$ and at $x \to \infty$, respectively.

In view of Eqs. (2.13)–(2.15), the total interaction force, F_x, can be expressed in two alternative forms:

$$F_x \equiv F_x^{(p)} + F_x^{(\gamma)} = F_x^{(S)} + F_x^{(C)} \tag{2.17}$$

$F_x^{(p)}$ and $F_x^{(\gamma)}$ are integrals over the particle surface and the contact line on the particle surface, whereas $F_x^{(S)}$ and $F_x^{(C)}$ are related to integrals over the surface and line on the midplane $x = 0$; see Fig. 4. In other words, there are two equivalent approaches for calculation of F_x: (i) by integration over the particle surface [16] and (ii) by integration over the midplane [75]. Depending on the specific problem, we could use that approach, which is more convenient. In general, $F_x^{(p)} \neq F_x^{(S)}$ and $F_x^{(\gamma)} \neq F_x^{(C)}$, the difference between them being due to the integral over S_{EFMN} in Eqs. (2.7) and (2.11).

It should be noted that the calculation of the force acting on the right-hand side particle by integration over the midplane is equivalent to an imaginary "freezing" of the right half-space and calculating the net force acting on the midplane from the side of the left half-space. Furthermore, Eqs. (2.1) and (2.7), together with the respective three- and two-dimensional divergence theorems lead to the conclusion that the net force acting on the midplane is equal to the force exerted on the right-hand-side particle; see Eq. (2.17). Thus, the problem for calculating F_x can be reduced to the calculation of the meniscus shape, $z = \zeta(x,y)$, and of the pressure tensor, $\mathbf{P}$, *only* in the midplane $x = 0$; see Eqs. (2.13)–(2.15). This is a very important result because in the *middle* between the particles the meniscus slope is small, even if it is not small close to the particles. This fact allows us to considerably simplify the problem because of the following two reasons. Firstly, for small meniscus slope the square root in Eq. (2.14) can be expanded in series:

$$F_x^{(C)} = \frac{\gamma}{2}\int\limits_{-\infty}^{\infty} dy\left(\zeta_x^2-\zeta_y^2\right)\Big|_{x=0}. \tag{2.18}$$

Secondly, in the region of small slope the Laplace equation of capillarity can be linearized. Hence, in this region the meniscus shape can be expressed as a superposition of the menisci created by the two particles in isolation:

$$\zeta(x,y) = \zeta_A(x,y) + \zeta_B(x,y) \quad (\text{in the midplane } x = 0) \tag{2.19}$$

where ζ_A is the meniscus created by the left-hand-side particle if the other particle was missing, and ζ_B is the meniscus created by the right-hand-side particle if the other particle was missing. Eq. (2.19) expresses a superposition approximation, which is applicable in all cases when the meniscus slope is small in the *middle* between the particles. (It is not necessary the slope to be small near the particles!) This approximation considerably simplifies the problem. It is worthwhile noting that a similar approximation was used by Verwey and Overbeek [77] to derive their known expression for the electrostatic disjoining pressure. For capillary forces, this approach was first applied in Ref. [75].

2.2. Case of noncharged particles at a liquid interface

The general expressions derived in Section 2.1 can be applied to systems where gravitational and/or electric fields are present. Hereafter, we will consider the special case with gravitational field alone, i.e. two noncharged particles floating on a horizontal liquid interface. In such case, the pressure tensor is isotropic in the two neighboring phases, I and II:

$$\mathbf{P}_I = (p_\infty-\rho_I gz)\mathbf{U} \ \text{ and } \ \mathbf{P}_{II} = (p_\infty-\rho_{II}gz)\mathbf{U} \tag{2.20}$$

where p_∞ is the pressure at level $z = 0$; $\mathbf{U}$ is the spatial unit tensor; ρ_I and ρ_{II} are the mass densities of the respective phases. Substituting Eq. (2.20) into Eq. (2.16), we obtain:

$$F_x^{(S)} = \int\limits_{-\infty}^{\infty} dy\int\limits_{0}^{\zeta} dz(p_\infty-\rho_I gz) - \int\limits_{-\infty}^{\infty} dy\int\limits_{0}^{\zeta} dz(p_\infty-\rho_{II}gz) = -\int\limits_{-\infty}^{\infty} dy\int\limits_{0}^{\zeta} dz(\rho_I-\rho_{II})gz = -\frac{1}{2}\gamma q^2\int\limits_{-\infty}^{\infty} dy\zeta^2 \tag{2.21}$$

where q is the inverse capillary length in Eq. (1.2) with

$$\Delta\rho = \rho_I-\rho_{II}. \tag{2.22}$$

Combining Eqs. (2.13), (2.18) and (2.21), we obtain [75]:

$$F_x = -\frac{\gamma}{2}\int\limits_{-\infty}^{\infty} dy\left[q^2\zeta^2 + \left(\frac{\partial\zeta}{\partial y}\right)^2 - \left(\frac{\partial\zeta}{\partial x}\right)^2\right]\Bigg|_{x=0} \tag{2.23}$$

Because we are using the assumption for small meniscus slope in the midplane, $x = 0$, we can substitute the superposition approximation, Eq. (2.19), into Eq. (2.23):

$$F_x = -\gamma\int\limits_{-\infty}^{\infty} dy\left(q^2\zeta_A\zeta_B + \frac{\partial\zeta_A}{\partial y}\frac{\partial\zeta_B}{\partial y} - \frac{\partial\zeta_A}{\partial x}\frac{\partial\zeta_B}{\partial x}\right)\Bigg|_{x=0} \tag{2.24}$$

To derive Eq. (2.24), we have used the fact that the forces $F_x^{(A)}$ and $F_x^{(B)}$ acting on the *isolated* particles A and B, are equal to zero:

$$F_x^{(Y)} = -\frac{\gamma}{2}\int\limits_{-\infty}^{\infty} dy\left[q^2\zeta_Y^2 + \left(\frac{\partial\zeta_Y}{\partial y}\right)^2 - \left(\frac{\partial\zeta_Y}{\partial x}\right)^2\right]\Bigg|_{x=0} = 0,\ Y = A,B \tag{2.25}$$

As known [1,10–12,78], the meniscus profiles around the separate particles are described by the expressions:

$$\zeta_A = -Q_A K_0(q\rho_A), \quad \zeta_B = -Q_B K_0(q\rho_B) \tag{2.26}$$

where ρ_A and ρ_B are the distances from a given point in the xy-plane to the centers of particles A and B (see Fig. 1); the coefficients Q_A and Q_B are the so called 'capillary charges' [11,78]:

$$Q_Y = r_Y\sin\psi_Y,\ \sin\psi_Y \approx \tan\psi_Y = \frac{d\zeta_Y}{dr}\Big|_{r=r_Y},\ Y = A,B \tag{2.27}$$

r_Y is the radius of the contact lines on the surface of particle Y ($Y=A$, B), see Fig. 1; ψ_Y is the meniscus slope angle at the particle contact line.

In Ref. [75], numerical solution of the integral in Eq. (2.24), along with Eq. (2.26), was carried out for two equal-sized particles, and it was found that the *numerical* results for F_x exactly coincide with the prediction of the known formula [1,10–12,78]:

$$F_x = -2\pi\gamma Q_A Q_B q K_1(qL) \tag{2.28}$$

Here, F_x is the x-projection of the force acting on the right-hand side particle. The equivalence of Eqs. (2.24) and (2.26) to the asymptotic formula Eq. (2.28) has not yet been proven *analytically*. Below, we will prove that really Eq. (2.28) is an exact corollary of Eqs. (2.24) and (2.26). For this goal, we have to first introduce the tensor of capillary interaction (Section 2.3). The developed method will further help us to derive analogous expressions for the interaction between two capillary multipoles of arbitrary order.

2.3. Calculation of capillary force by integrating the tensor of capillary interaction

In the case of small interfacial slope, the meniscus profiles ζ_A and ζ_B obey the linearized Laplace equations of capillarity:

$$\frac{\partial^2\zeta_Y}{\partial x^2} + \frac{\partial^2\zeta_Y}{\partial y^2} = q^2\zeta_Y \ (Y = A, B). \tag{2.29}$$

It is convenient to introduce the notations:

$$x_1 \equiv x \quad \text{and} \quad x_2 \equiv y. \tag{2.30}$$

Next, let us define the symmetric two-dimensional tensor T_{kn} as follows:

$$T_{kn} \equiv \frac{\partial\zeta_A}{\partial x_k}\frac{\partial\zeta_B}{\partial x_n} + \frac{\partial\zeta_A}{\partial x_n}\frac{\partial\zeta_B}{\partial x_k} - \left(\frac{\partial\zeta_A}{\partial x_j}\frac{\partial\zeta_B}{\partial x_j} + q^2\zeta_A\zeta_B\right)\delta_{kn} \tag{2.31}$$

($k,n=1,2$) where δ_{kn} is the two-dimensional Kronecker symbol and summation is assumed over the repeated index j (the Einstein rule). By using Eq. (2.29), we find that the divergence of the tensor T_{kn} is equal to zero:

$$\frac{\partial T_{kn}}{\partial x_k} = 0, \ n = 1,2 \tag{2.32}$$

i.e. $\nabla\cdot\mathbf{T}=\mathbf{0}$, in tensorial notations. Further, we integrate Eq. (2.32) over a domain S_+, which represents the right half of the xy-plane (corresponding to $x>0$), except a circle, C_δ, around the center of particle B (Fig. 1), and use the Green theorem:

$$\mathbf{0} = -\int_{S_+} dS\nabla\cdot\mathbf{T} = \int_{-\infty}^{\infty} dy\mathbf{e}_x\cdot\mathbf{T}|_{x=0} + \int_{C_\delta} d\mathbf{l}_\delta\cdot\mathbf{T} \tag{2.33}$$

where $\mathbf{n}_\delta$ is the outer unit normal field of the contour C_δ. Taking the x-projection of the latter equation, in view of Eq. (2.31) we derive:

$$\int_{-\infty}^{\infty} dy\left(q^2\zeta_A\zeta_B + \frac{\partial\zeta_A}{\partial y}\frac{\partial\zeta_B}{\partial y} - \frac{\partial\zeta_A}{\partial x}\frac{\partial\zeta_B}{\partial x}\right)\Bigg|_{x=0} = \int_{C_\delta} d\mathbf{l}_\delta\cdot\mathbf{T}\cdot\mathbf{e}_x \tag{2.34}$$

Finally, in view of Eqs. (2.24) and (2.34) we obtain:

$$F_x = -\gamma\int_{C_\delta} d\mathbf{l}_\delta\cdot\mathbf{T}\cdot\mathbf{e}_x \tag{2.35}$$

The covariant form of the tensor of capillary interaction defined by Eq. (2.31) is:

$$\mathbf{T} = (\nabla\zeta_A)\nabla\zeta_B + (\nabla\zeta_B)\nabla\zeta_A - \left[(\nabla\zeta_A)\cdot\nabla\zeta_B + q^2\zeta_A\zeta_B\right]\mathbf{U} \tag{2.36}$$

In Section 3, Eqs. (2.35) and (2.36) will be used for calculating the force of capillary interaction between various capillary multipoles, including capillary charges ($m=0$); dipoles ($m=1$); quadrupoles ($m=2$); hexapoles ($m=3$), etc.; see Eq. (1.4).

3. Forces of interaction between capillary multipoles

3.1. Integral expression for the capillary force

Here, we will use polar coordinates (ρ_A,ϕ_A) and (ρ_B,ϕ_B) associated, respectively, with the left- and right-hand-side particle (Fig. 1):

$$x \equiv -\frac{L}{2} + \rho_A\cos\phi_A \quad \text{and} \quad y \equiv \rho_A\sin\phi_A \tag{3.1}$$

$$x \equiv \frac{L}{2} - \rho_B\cos\phi_B \quad \text{and} \quad y \equiv \rho_B\sin\phi_B. \tag{3.2}$$

Then, the expression for the force acting on the right-hand-side particle, Eq. (2.35), can be represented in the form:

$$F_x = -\gamma r_\delta\int_0^{2\pi} d\phi_B\mathbf{e}_\rho\cdot\mathbf{T}\cdot\mathbf{e}_x \quad \text{at} \quad \rho_B = r_\delta \tag{3.3}$$

where $\mathbf{e}_\rho$ is a radial unit vector; r_δ is the radius of the contour C_δ (see Fig. 1). The tensor T_{kn} in Eq. (2.31) contains the functions ζ_A and ζ_B, and their derivatives. To carry out the integration in Eq. (3.3), we will use the polar coordinates (ρ_B,ϕ_B) defined by Eq. (3.2). Differentiating the two expressions in Eq. (3.2), we find:

$$\left(\frac{\partial\rho_B}{\partial x}\right)_y = -\cos\phi_B \quad \text{and} \quad \left(\frac{\partial\phi_B}{\partial x}\right)_y = \frac{\sin\phi_B}{\rho_B} \tag{3.4}$$

Further, with the help of Eq. (3.4) we obtain:

$$\frac{\partial\zeta_Y}{\partial x} = -\frac{\partial\zeta_Y}{\partial\rho_B}\cos\phi_B + \frac{\partial\zeta_Y}{\partial\phi_B}\frac{\sin\phi_B}{\rho_B}, \ Y = A, B. \tag{3.5}$$

The substitution of the tensor $\mathbf{T}$ from Eq. (2.36) into Eq. (3.3), in view of Eq. (3.5) yields:

$$F_x = \gamma r_\delta\int_0^{2\pi}\left[\frac{\partial\zeta_A}{\partial\rho_B}\frac{\partial\zeta_B}{\partial\rho_B}\cos\phi_B - \left(\frac{\partial\zeta_A}{\partial\phi_B}\frac{\partial\zeta_B}{\partial\rho_B} + \frac{\partial\zeta_A}{\partial\rho_B}\frac{\partial\zeta_B}{\partial\phi_B}\right)\frac{\sin\phi_B}{r_\delta} - \left(\frac{1}{r_\delta^2}\frac{\partial\zeta_A}{\partial\phi_B}\frac{\partial\zeta_B}{\partial\phi_B} + q^2\zeta_A\zeta_B\right)\cos\phi_B\right]d\phi_B \text{ at } \rho_B = r_\delta \tag{3.6}$$

where the relationship $\mathbf{e}_\rho\cdot\mathbf{e}_x = -\cos\phi_B$ (see Fig. 1) has been used.

3.2. Interaction of a capillary charge with capillary multipoles

First, let us assume that particle B is a capillary charge. Then, only the term with $m=0$ remains in the Fourier expansion for ζ_B in Eq. (1.3). In such a case, we have $\zeta_B = \zeta_B(\rho_B)$; all terms containing the derivative $\partial\zeta_B/\partial\phi_B$ disappear, and Eq. (3.6) reduces to

$$F_x = \gamma r_\delta\int_0^{2\pi}\left[\left(\frac{\partial\zeta_A}{\partial\rho_B}\cos\phi_B - \frac{\partial\zeta_A}{\partial\phi_B}\frac{\sin\phi_B}{\rho_B}\right)\frac{\partial\zeta_B}{\partial\rho_B} - q^2\zeta_A\zeta_B\cos\phi_B\right]d\phi_B \text{ at } \rho_B = r_\delta. \tag{3.7}$$

Eq. (3.7) is a special case of Eq. (2.35). The way of derivation of Eq. (2.35) implies that F_x must be the same independently of the

choice of r_δ. Here, we will use the transition $r_\delta \to 0$, which is possible because the Fourier expansion of the meniscus profile, Eqs. (1.3)–(1.4), defines the functions $\zeta_A(\rho_A,\phi_A)$ and $\zeta_B(\rho_B,\phi_B)$ in the whole xy-plane. As demonstrated below, the pole of ζ_A at $\rho_A = 0$ and the pole of ζ_B at $\rho_B = 0$ do not represent an obstacle for the derivation of expressions for the capillary forces; see e.g. Eq. (3.9). The limiting transition $r_\delta \to 0$ is equivalent to the method of residues applied in Ref. [34]. The present method is simpler because it avoids using mathematical analysis in terms of functions of complex variables.

Thus, in Eq. (3.7) we apply the limiting transition $r_\delta \to 0$, and use Eq. (3.5) and the fact that $\zeta_B = -Q_B K_0(q\rho_B)$:

$$F_x = -2\pi\gamma\left[\frac{\partial\zeta_A}{\partial x}\left(r_\delta\frac{\partial\zeta_B}{\partial\rho_B}\right)\right]\Bigg|_{\rho_B = r_\delta \to 0} \tag{3.8}$$

In view of Eq. (2.26), we derive:

$$\left(r_\delta\frac{\partial\zeta_B}{\partial\rho_B}\right)\Bigg|_{\rho_B = r_\delta \to 0} = -Q_B\left[r_\delta\frac{\partial K_0(q\rho_B)}{\partial\rho_B}\right]\Bigg|_{\rho_B = r_\delta \to 0} = Q_B \tag{3.9}$$

where we have used the mathematical relations [68,69,79]:

$$\frac{dK_0(x)}{dx} = -K_1(x) \quad \text{and} \quad K_1(x) \approx \frac{1}{x} \quad \text{for} \quad x \to 0. \tag{3.10}$$

The substitution of Eq (3.9) in Eq. (3.8) yields:

$$F_x = -2\pi\gamma Q_B\left(\frac{\partial\zeta_A}{\partial x}\right)\Bigg|_{r_\delta \to 0} \tag{3.11}$$

From Eq. (3.1) we derive:

$$\rho_A^2 = \left(\frac{L}{2} + x\right)^2 + y^2 \quad \text{and} \quad \tan\phi_A = \frac{2y}{L + 2x} \tag{3.12}$$

$$\frac{\partial\rho_A}{\partial x} = \frac{x + L/2}{\rho_A} \quad \text{and} \quad \frac{\partial\phi_A}{\partial x} = -\frac{y\cos^2\phi_A}{(x + L/2)^2}. \tag{3.13}$$

For $r_\delta \to 0$, we have $x \to L/2$, $y \to 0$, $\rho_A \to L$ and $\phi_A \to 0$. Hence,

$$\frac{\partial\rho_A}{\partial x}\Bigg|_{r_\delta \to 0} = 1 \quad \text{and} \quad \frac{\partial\phi_A}{\partial x}\Bigg|_{r_\delta \to 0} = 0. \tag{3.14}$$

Assuming that the particle A is a *capillary charge*, i.e. $\zeta_A = -Q_A K_0(q\rho_A)$, with the help of Eqs. (3.10) and (3.14) we derive:

$$\left(\frac{\partial\zeta_A}{\partial x}\right)\Bigg|_{r_\delta \to 0} = \frac{\partial}{\partial\rho_A}[-Q_A K_0(q\rho_A)]\Bigg|_{r_\delta \to 0} = qQ_A K_1(qL). \tag{3.15}$$

The substitution of Eq. (3.15) into Eq. (3.11) gives exactly the known asymptotic formula for the capillary force, Eq. (2.28). This result proves that Eq. (2.28) can be analytically deduced from Eq. (2.24). We recall that Eq. (3.3) is equivalent to Eq. (2.24).The comparison of Eq. (1.4) for $m = 0$ with Eq. (2.26) yields:

$$Q_Y \equiv -\frac{h_{Y,0}}{K_0(qr_Y)}, \quad Y = A, B. \tag{3.16}$$

Substituting Eq. (3.16) into Eq. (2.28), we obtain:

$$F_x = -\pi\gamma q h_{A,0} h_{B,0}\frac{K_1(qL) + K_{-1}(qL)}{K_0(qr_A)K_0(qr_B)} \text{ (charge – charge)} \tag{3.17}$$

where we have used the identity $K_1(qL) = K_{-1}(qL)$ [68,69,79]. The latter presentation of the force between two capillary charges ($m = 0$) is useful, because it allows generalization for capillary multipoles of arbitrary order; see Eqs. (3.20) and (3.27) below.

Furthermore, if the particle A is a *capillary multipole* of order m, while the particle B is a capillary charge ($m = 0$), as before, from Eqs. (1.4), (3.11) and (3.14), we derive:

$$\left(\frac{\partial\zeta_A}{\partial x}\right)\Bigg|_{r_\delta \to 0} = \frac{\partial}{\partial x}\left\{h_{A,m}\frac{K_m(q\rho_A)}{K_m(qr_A)}\cos\left[m\left(\phi_A - \phi_{A,m}\right)\right]\right\}\Bigg|_{\rho_B = r_\delta \to 0} \tag{3.18}$$
$$= -\frac{qh_{A,m}}{2}\frac{K_{m+1}(qL) + K_{m-1}(qL)}{K_m(qr_A)}\cos\left(m\phi_{A,m}\right)$$

where we have used Eq. (3.14) and the relation [68,69,80]:

$$\frac{dK_m}{dx} = -\frac{1}{2}\left[K_{m+1}(x) + K_{m-1}(x)\right]. \tag{3.19}$$

Substituting Eq. (3.18) into Eq. (3.11), we obtain the expression for the force of interaction between a capillary charge and a capillary multipole of order m:

$$F_x = -\pi\gamma q h_{A,m} h_{B,0}\frac{K_{m+1}(qL) + K_{m-1}(qL)}{K_m(qr_A)K_0(qr_B)}\cos\left(m\phi_{A,m}\right) \text{ (charge – multipole)} \tag{3.20}$$

($m = 0, 1, 2, \ldots$) where Eq. (3.16) has been used for $Y = B$. Eq. (3.20) gives accurately the dependence $F_x(L)$ for all L-values, for which the meniscus slope in the middle between the two particles is small, i.e. $((\partial\zeta/\partial x)^2 + (\partial\zeta/\partial y)^2)_{x=0} \ll 1$, so that the Young–Laplace equation can be linearized at the midplane. Substituting $m = 0$ in Eq. (3.20), we obtain Eq. (3.17), as it should be expected. Furthermore, integrating Eq. (3.20) with respect to L and using Eq. (3.19), we obtain an expression for the interaction energy:

$$\Delta W = 2\pi\gamma h_{A,m} Q_B\frac{K_m(qL)}{K_m(qr_A)}\cos\left(m\phi_{A,m}\right) \text{ (charge – multipole)} \tag{3.21}$$

($m = 0, 1, 2, \ldots$) where Eq. (3.16) has been used again for $Y = B$.

In the asymptotic case $qL \ll 1$ (and $qr_A \ll 1$), using Eq. (1.5) we can simplify Eq. (3.20):

$$F_x \approx 2m\pi\gamma h_{A,m} Q_B\frac{r_A^m}{L^{m+1}}\cos\left(m\phi_{A,m}\right) \text{ (charge – multipole for } qL \ll 1) \tag{3.22}$$

which is valid for $m \geq 1$. Integrating Eq. (3.22) we obtain the respective asymptotic expression for the energy of capillary interaction:

$$\Delta W \approx 2\pi\gamma h_{A,m} Q_B\frac{r_A^m}{L^m}\cos\left(m\phi_{A,m}\right) \text{ (charge – multipole for } qL \ll 1) \tag{3.23}$$

($m = 1, 2, \ldots$). Eq. (3.23) is the correct asymptotics of $\Delta W(L)$. In our previous paper, Ref. [34] (see Table 2 therein), the factor 2π in the right-hand side of Eq. (3.23) was given (by mistake) as $\pi/2$.

3.3. Interactions between capillary multipoles of arbitrary order

Here, we consider the case where the particle A is a capillary multipole of order m, whereas the particle B is a capillary multipole of order n ($m, n = 1, 2, \ldots$); see also Fig. 1. Because we will use the limiting transition $\rho_B = r_\delta \to 0$ in Eq. (3.6), we can work, from the very beginning, with the expression for ζ_B in its form for small ρ_B:

$$\zeta_B(x,y) \approx \frac{h_{B,n}}{K_n(qr_B)}\frac{2^{n-1}(n-1)!}{(q\rho_B)^n}\cos\left[n\left(\phi_B - \phi_{B,n}\right)\right] \text{ for } n \geq 1 \tag{3.24}$$

see Eqs. (1.4) and (1.5). Substituting Eq. (3.24) into Eq (3.6), after some mathematical transformations we obtain:

$$F_x = -\frac{2^{n-1}\gamma h_{B,n}}{q^n K_n(qr_B)}\int_0^{2\pi}\frac{n!}{r_\delta^n}\left[\frac{\partial\zeta_A}{\partial\rho_B}+\frac{n+1}{r_\delta}\zeta_A\right]\Big|_{\rho_B=r_\delta} \cos\left[(n+1)\phi_B-n\phi_{B,n}\right]d\phi_B. \tag{3.25}$$

Next, in Eq. (3.25) we substitute the expression for ζ_A from Eq. (1.4), and after some transformations using the transition $\rho_B=r_\delta\to 0$ we derive (see Appendix B):

$$F_x = -\frac{2^n\gamma h_{A,m}h_{B,n}}{q^n K_m(qr_A)K_n(qr_B)}\int_0^{2\pi}\frac{\partial^{n+1}}{\partial\rho_B^{n+1}}\left\{K_m(q\rho_A)\cos\left[m\left(\phi_A-\phi_{A,m}\right)\right]\right\}\Big|_{\rho_B=0} \times\cos\left[(n+1)\phi_B-n\phi_{B,n}\right]d\phi_B \tag{3.26}$$

From Eq. (3.26), after some calculations described in Appendix C, we derive the general expression for the force of interaction between two capillary multipoles of orders m and n:

$$F_x = -\frac{\pi\gamma q h_{A,m}h_{B,n}}{2K_m(qr_A)K_n(qr_B)}\left[K_{m+n+1}(qL)\cos\left(m\phi_{A,m}-n\phi_{B,n}\right) + K_{m-n-1}(qL)\cos\left(m\phi_{A,m}+n\phi_{B,n}\right)\right] \tag{3.27}$$

$(m, n=1, 2, 3, \ldots)$. Eq. (3.27) gives accurately the dependence $F_x(L)$ for all L-values, for which the meniscus slope in the middle between the two particles is small, i.e. $(\zeta_x^2+\zeta_y^2)_{x=0}\ll 1$, so that the Young–Laplace equation can be linearized at the midplane. In the case of small particles, $qL\ll 1$, with the help of Eq. (1.5) we obtain the asymptotic form of Eq. (3.27):

$$F_x\approx -2\pi\frac{(m+n)!}{(m-1)!(n-1)!}\gamma h_{A,m}h_{B,n}\frac{r_A^m r_B^n}{L^{m+n+1}}\cos\left(m\phi_{A,m}-n\phi_{B,n}\right)\ \text{for}\ qL\ll 1. \tag{3.28}$$

Integrating Eq. (3.28) with respect to L, we obtain the energy of capillary interaction between m- and n-multipoles given by Eq. (1.7).

Eq. (3.27) is more general than Eq. (3.28), because the latter represents a special case for $qL\ll 1$. The capillary interaction energy, ΔW, obtained by integration of the general Eq. (3.27), is:

$$\Delta W = -\frac{\pi\gamma h_{A,m}h_{B,n}}{2K_m(qr_A)K_n(qr_B)}\left[G_{m+n+1}(qL)\cos\left(m\phi_{A,m}-n\phi_{B,n}\right) + G_{m-n-1}(qL)\cos\left(m\phi_{A,m}+n\phi_{B,n}\right)\right] \tag{3.29}$$

where $m, n=1, 2, \ldots$, and

$$G_j(qL)\equiv\int_{qL}^{\infty}K_j(\xi)d\xi,\qquad j=0,\pm 1,\pm 2,\ldots \tag{3.30}$$

where ξ is an integration variable. For $qL\ll 1$, Eq. (3.29) reduces to Eq. (1.7). For calculation of the functions $G_j(x)$ in Eq. (3.29), one can use the following procedure.

Because $K_{-j}(x)=K_j(x)$, Eq. (3.30) implies that $G_{-j}(x)=G_j(x)$. Hence, the problem reduces to calculation of $G_j(x)$ for nonnegative integer values of j. For $j=0$ and 1 we have:

$$G_0(x) = \frac{\pi}{2}[1-xK_0(x)\boldsymbol{L}_{-1}(x)-xK_1(x)\boldsymbol{L}_0(x)] \tag{3.31}$$

$$G_1(x) = K_0(x) \tag{3.32}$$

where $\boldsymbol{L}_n(x), n=0, \pm 1, \pm 2, \ldots$, is the modified Struve function [79,82,83]. The modified Struve and Bessel functions $\boldsymbol{L}_{-1}(x)$, $\boldsymbol{L}_0(x)$, $K_0(x)$, $K_1(x)$, …, can be quickly and accurately calculated by using computational software programs, such as 'Mathematica' developed by Wolfram Research (Illinois, USA). Further, we have:

$$G_2(x) = 2K_1(x)-G_0(qL) \tag{3.33}$$

and so on. In general, the following recurrence formula holds (Appendix C):

$$G_j(x) = 2K_{j-1}(x)-G_{j-2}(x),\qquad j=2,\ 3,\ldots \tag{3.35}$$

Note that for small values of x, Eq. (3.35) predicts that $G_j(x)\approx 2K_{j-1}(x)$. Additional information can be found at the end of Appendix C.

It should be noted that Eqs. (3.27) and (3.29) have asymptotic character. At $L/(2r_c)<1.5$, they predict a stronger attraction than the real one as indicated by their comparison with the exact solution of the problem in bipolar coordinates at short distances; see Fig. 6 in Ref. [33] and Fig. 7 in Ref. [34]. This inaccuracy originates from the fact that the superposition approximation for the meniscus shape in the middle between the two particles, Eq. (2.19), becomes less accurate at short interparticle distances. Note however that Eqs. (3.27) and (3.29) are very accurate for $L/(2r_c)>1.5$, and their accuracy increases with the rise of interparticle separation. They represent compact expressions, which are much easier for applications than the solutions in terms of bipolar coordinates in Refs. [33,34].

It should be also noted that Eq. (3.28), and its integrated form, Eq. (1.7), exactly coincide with the respective result in Ref. [34] obtained by solving the problem in bipolar coordinates without using any superposition approximation. This result confirms the validity of the special version of the superposition approximation, Eq. (2.19), which has been applied here *only* in the midplane between the two particles.

4. Summary and concluding remarks

The liquid interface around an adsorbed colloidal particle can be undulated because of roughness or heterogeneity of the particle surface, or due to the fact that the particle has a non-spherical (e.g. ellipsoidal or polyhedral) shape. In such case, the meniscus around the particle can be expanded in Fourier series, which is equivalent to a linear combination of capillary multipoles, namely, capillary charges, dipoles, quadrupoles, etc.; see Eqs. (1.3) and (1.4). The capillary multipoles attract a growing interest because their interactions have been found to influence the self-assembly of particles at liquid interfaces, as well as the interfacial rheology and the properties of particle-stabilized foams and emulsions. As a rule, the interfacial deformations in the middle between two adsorbed particles are small. This fact can be used for derivation of accurate asymptotic expressions for calculating the capillary forces by integration in the midplane, where the Young–Laplace equation can be linearized and the superposition approximation can be applied. We utilized this approach to derive a general integral expression for the capillary force; see Eqs. (2.13)–(2.15). It is applicable to the cases when gravitational and electric fields (e.g. due to charged particles) are present in the system. In the special case of gravity field alone, the derived integral expression reduces to a formula obtained in Ref. [75]; see Eq. (2.23).

It is a nontrivial task to obtain convenient analytical formulas for the capillary forces from the derived integral expression. We developed a new theoretical approach based on the tensor of capillary interactions; see Eqs. (2.31) and (2.36). It has been applied by us to derive explicit asymptotic expressions for the force between a capillary charge and a capillary multipole, Eqs. (3.20) and (3.21), and between two capillary multipoles of arbitrary order, Eqs. (3.27) and (3.29). The obtained expressions are more general that the previously published ones [34], the validity of the latter being limited to sufficiently small interparticle distances, $qL\ll 1$. Note also that in Ref. [34] we used the energy approach, i.e. ΔW was calculated, and then the force F_x was obtained by differentiation. In contrast, in the

present article we are using the force approach, which is based on the calculation of F_x, and then we obtain the interaction energy, ΔW, by integration. Of course, if correctly applied, the two approaches yield identical results.

Acknowledgements

Support from the National Science Fund of Bulgaria, grant number DO-02-121/2009, and a partial support from EU COST Action D43 "Colloid and Interface Chemistry for Nanotechnology" are gratefully acknowledged.

Appendix A. Calculation of the meniscus shape

The meniscus shape around the particles $z=\zeta(x,y)$ obeys Eq. (1.1), where the right-hand side can be neglected for $q(x^2+y^2)^{1/2}\ll 1$. Explicit expression for $\zeta(x,y)$ is obtained in Ref. [34] in terms of the bipolar coordinates, τ and ω, in the xy-plane:

$$x=\frac{a\sinh\tau}{\cosh\tau-\cos\omega}\ ,\ y=\frac{a\sin\omega}{\cosh\tau-\cos\omega} \tag{A.1}$$

where a is a parameter related to the radii of the two contact lines, r_A and r_B, and the interparticle distance L through the equation [33,34]:

$$a=\frac{1}{2L}\left[L^2-(r_A+r_B)^2\right]^{1/2}\left[L^2-(r_A-r_B)^2\right]^{1/2}. \tag{A.2}$$

The projections of the two contact lines on the xy-plane correspond to $\tau=-\tau_A$ and $\tau=\tau_B$ defined as

$$\tau_A=\operatorname{arccosh}\left(\frac{L^2+r_A^2-r_B^2}{2Lr_A}\right) \tag{A.3}$$

$$\tau_B=\operatorname{arccosh}\left(\frac{L^2+r_B^2-r_A^2}{2Lr_B}\right) \tag{A.4}$$

$$\operatorname{arccosh}\ \xi\equiv\ln\left[\xi+\left(\xi^2-1\right)^{1/2}\right]. \tag{A.5}$$

To calculate the meniscus shape $z=\zeta(x,y)$, for given x and y we first calculate:

$$d_A=\left[(x+a)^2+y^2\right]^{1/2}, d_B=\left[(x-a)^2+y^2\right]^{1/2} \tag{A.6}$$

$$\tau=\ln\left(\frac{d_A}{d_B}\right), \omega=\arccos\left(\frac{d_A^2+d_B^2-4a^2}{2d_Ad_B}\right) \tag{A.7}$$

where $\omega\geq 0$ for $y\geq 0$, and $\omega<0$ for $y<0$. Next, the meniscus profile is calculated from the following series [34]:

$$\begin{aligned}\zeta=\ & h_{A,m}(-1)^m\sum_{k=1}^{\infty}A(k,m,\tau_A)\cos\left(k\omega+m\phi_{A,m}\right)\frac{\sinh[k(\tau_B-\tau)]}{\sinh[k(\tau_A+\tau_B)]}\\ &+h_{B,m}(-1)^n\sum_{k=1}^{\infty}A(k,n,\tau_B)\cos\left(k\omega+n\phi_{B,n}\right)\frac{\sinh[k(\tau_A-\tau)]}{\sinh[k(\tau_A+\tau_B)]}\\ &+h_{A,m}\frac{\tau_B-\tau}{\tau_A+\tau_B}\exp(-m\tau_A)\cos\left(m\phi_{A,m}\right)\\ &+h_{B,n}\frac{\tau+\tau_A}{\tau_A+\tau_B}\exp(-n\tau_B)\cos\left(n\phi_{B,n}\right)\end{aligned} \tag{A.8}$$

where the coefficients are

$$A(k,j,\tau_Y)=\frac{1}{(j-1)!}\frac{d^{j-1}}{dt^{j-1}}\left[t^{k-1}(1-\beta t)^j\right]\Big|_{t=\beta} \tag{A.9}$$

$$\beta=\exp\left(-\tau_Y\right)\ (Y=A,B). \tag{A.10}$$

The first two sums in the right-hand side of Eq. (A.8) correspond to Eq. (3.20) in Ref. [34]. (The phase-shift angles in Ref. [34] are defined as $\pi-\phi_{Y,m}$, where $\phi_{Y,m}$ is the phase-shift angle in the present article.) The last two terms in Eq. (A.8), which do not depend on ω, have been omitted in Ref. [34], because they do not contribute to the interaction energy ΔW. However, they are important for the calculation of the meniscus shape $z=\zeta(x,y)$.

Appendix B. Derivation of an integral formula for the capillary forces

First, we represent Eq. (3.6) in the following equivalent form:

$$\begin{aligned}F_x=\gamma r_\delta\int_0^{2\pi}\Bigg[&\frac{\partial\zeta_A}{\partial\rho_B}\left(\frac{\partial\zeta_B}{\partial\rho_B}\cos\phi_B-\frac{\partial\zeta_B}{\partial\phi_B}\frac{\sin\phi_B}{r_\delta}\right)-q^2\zeta_A\zeta_B\cos\phi_B\\ &-\frac{\partial\zeta_A}{\partial\phi_B}\left(\frac{\partial\zeta_B}{\partial\rho_B}\frac{\sin\phi_B}{r_\delta}+\frac{\partial\zeta_B}{\partial\phi_B}\frac{\cos\phi_B}{r_\delta^2}\right)\Bigg]d\phi_B\ \text{ at }\ \rho_B=r_\delta.\end{aligned} \tag{B.1}$$

Integrating by parts the last term in Eq. (B.1), we derive:

$$\begin{aligned}F_x=\gamma r_\delta\int_0^{2\pi}\Bigg[&\frac{\partial\zeta_A}{\partial\rho_B}\left(\frac{\partial\zeta_B}{\partial\rho_B}\cos\phi_B-\frac{\partial\zeta_B}{\partial\phi_B}\frac{\sin\phi_B}{r_\delta}\right)-q^2\zeta_A\zeta_B\cos\phi_B\\ &+\zeta_A\frac{\partial}{\partial\phi_B}\left(\frac{\partial\zeta_B}{\partial\rho_B}\frac{\sin\phi_B}{r_\delta}+\frac{\partial\zeta_B}{\partial\phi_B}\frac{\cos\phi_B}{r_\delta^2}\right)\Bigg]d\phi_B\ \text{ at }\ \rho_B=r_\delta.\end{aligned} \tag{B.2}$$

Using Eq. (1.1) for $Y=B$, we bring Eq. (B.2) to the form:

$$\begin{aligned}F_x=\gamma r_\delta\int_0^{2\pi}\Bigg[&\frac{\partial\zeta_A}{\partial\rho_B}\left(\frac{\partial\zeta_B}{\partial\rho_B}\cos\phi_B-\frac{\partial\zeta_B}{\partial\phi_B}\frac{\sin\phi_B}{r_\delta}\right)\\ &+\zeta_A\left(\frac{\partial^2\zeta_B}{\partial\rho_B\partial\phi_B}\frac{\sin\phi_B}{r_\delta}-\frac{\partial\zeta_B}{\partial\phi_B}\frac{\sin\phi_B}{r_\delta^2}-\frac{\partial^2\zeta_B}{\partial\rho_B^2}\cos\phi_B\right)\Bigg]d\phi_B\ \text{ at }\ \rho_B=r_\delta.\end{aligned} \tag{B.3}$$

Substituting ζ_B from Eq. (3.24) in the right-hand side of Eq. (B.3), after some transformations we derive:

$$\begin{aligned}F_x=&-\frac{2^{n-1}\gamma h_{B,n}}{q^nK_n(qr_B)}\int_0^{2\pi}\left[\frac{n!}{r_\delta^n}\frac{\partial\zeta_A}{\partial\rho_B}+\frac{(n+1)!}{r_\delta^{n+1}}\zeta_A\right]\Bigg|_{\rho_B=r_\delta}\\ &\cos\left[(n+1)\phi_B-n\phi_{B,n}\right]d\phi_B.\end{aligned} \tag{B.4}$$

Further, we substitute the expression for ζ_A from Eq. (1.4) in the integrand of Eq. (B.4):

$$F_x=-\frac{2^{n-1}\gamma h_{A,m}h_{B,n}}{q^nK_m(qr_A)K_n(qr_B)}Z \tag{B.5}$$

where

$$Z\equiv\int_0^{2\pi}\left[\frac{n!}{r_\delta^n}\frac{\partial U}{\partial\rho_B}+\frac{(n+1)!}{r_\delta^{n+1}}U\right]\Bigg|_{\rho_B=r_\delta}\cos\left[(n+1)\phi_B-n\phi_{B,n}\right]d\phi_B \tag{B.6}$$

$$U(\rho_A,\phi_A)\equiv K_m(q\rho_A)\cos\left[m\left(\phi_A-\phi_{A,m}\right)\right]. \tag{B.7}$$

Next, we use a series expansion:

$$U(\rho_A,\phi_A)|_{\rho_B=r_\delta}=U(\rho_A,\phi_A)|_{\rho_B=0}+\sum_{k=1}^{\infty}\frac{\partial^kU}{\partial\rho_B^k}\Bigg|_{\rho_B=0}\frac{r_\delta^k}{k!}. \tag{B.8}$$

In view of Eq. (B.8), we obtain:

$$\left[\frac{n!}{r_\delta^n}\frac{\partial U}{\partial \rho_B}+\frac{(n+1)!}{r_\delta^{n+1}}U\right]\Bigg|_{\rho_B=r_\delta}=\left[\frac{n!}{r_\delta^n}\frac{\partial U}{\partial \rho_B}+\frac{(n+1)!}{r_\delta^{n+1}}U\right]\Bigg|_{\rho_B=0}+\frac{n!}{r_\delta^n}\sum_{k=1}^{\infty}\left.\frac{\partial^{k+1}U}{\partial \rho_B^{k+1}}\right|_{\rho_B=0}\frac{r_\delta^k}{k!}+\frac{(n+1)!}{r_\delta^{n+1}}\sum_{k=1}^{\infty}\left.\frac{\partial^k U}{\partial \rho_B^k}\right|_{\rho_B=0}\frac{r_\delta^k}{k!}. \quad (B.9)$$

In Appendix C, it is proven that the derivative $\partial^k U/\partial \rho_B^k$ at $\rho_B=0$ can be expanded in a *finite* Fourier series in terms of $\cos(j\phi_B)$ and $\sin(j\phi_B)$, where the maximum value of j is equal to the order of the derivative, that is $j\le k$. Therefore, in view of Eqs. (B.6) and (B.9) we have:

$$Z=\int_0^{2\pi}\left[\frac{n!}{r_\delta^n}\sum_{k=n}^{\infty}\left.\frac{\partial^{k+1}U}{\partial \rho_B^{k+1}}\right|_{\rho_B=0}\frac{r_\delta^k}{k!}+\frac{(n+1)!}{r_\delta^{n+1}}\sum_{k=n+1}^{\infty}\left.\frac{\partial^k U}{\partial \rho_B^k}\right|_{\rho_B=0}\frac{r_\delta^k}{k!}\right]\cos\left[(n+1)\phi_B-n\phi_{B,n}\right]d\phi_B. \quad (B.10)$$

Taking the limit of Eq. (B.10) for $r_\delta\to 0$, we obtain:

$$Z=\int_0^{2\pi}\left[\frac{n!}{r_\delta^n}\left.\frac{\partial^{n+1}U}{\partial \rho_B^{n+1}}\right|_{\rho_B=0}\frac{r_\delta^n}{n!}+\frac{(n+1)!}{r_\delta^{n+1}}\left.\frac{\partial^{n+1}U}{\partial \rho_B^{n+1}}\right|_{\rho_B=0}\frac{r_\delta^{n+1}}{(n+1)!}\right]\cos\left[(n+1)\phi_B-n\phi_{B,n}\right]d\phi_B$$

and finally

$$Z=2\int_0^{2\pi}\left.\frac{\partial^{n+1}U}{\partial \rho_B^{n+1}}\right|_{\rho_B=0}\cos\left[(n+1)\phi_B-n\phi_{B,n}\right]d\phi_B. \quad (B.11)$$

Combining Eqs. (B.5), Eq. (B.7) and (B.11), we obtain Eq. (3.26) in Section 3.3.

Appendix C. Obtaining an explicit expression for the capillary forces

Our goal here is to solve the integral in Eq. (3.26) and to derive the final formula for the multipole–multipole interaction, Eq. (3.27). For this goal, we will utilize the orthogonality of the sines and cosines [81]:

$$\int_0^{2\pi}\sin(m\phi)\sin(n\phi)d\phi=\int_0^{2\pi}\cos(m\phi)\cos(n\phi)d\phi=\pi\delta_{mn},\ n\neq 0 \quad (C.1)$$

$$\int_0^{2\pi}\sin(m\phi)\cos(n\phi)d\phi=0 \quad (C.2)$$

($m,n=0, 1, 2, \ldots$). The integrand in Eq. (3.26) contains $\cos[(n+1)\phi_B]$ as a multiplier, which means that only the $(n+1)$-mode of the Fourier expansion of the derivative in Eq. (3.26) will give a contribution to the capillary force, F_x. To find this mode, we will first prove that

$$\frac{2^k}{q^k}\frac{\partial^k}{\partial \rho_B^k}\left\{K_m(q\rho_A)\cos\left[m\left(\phi_A-\phi_{A,m}\right)\right]\right\}\Bigg|_{\rho_B=r_\delta\to 0} \quad (C.3)$$
$$=\sum_{j=0}^{k-1}\left[a_{j,k}\cos(j\phi_B)+b_{j,k}\sin(j\phi_B)\right]+K_{m+k}(qL)\cos\left(m\phi_{A,m}-k\phi_B\right)+K_{m-k}(qL)\cos\left(m\phi_{A,m}+k\phi_B\right)$$

where $a_{j,k}$ and $b_{j,k}$ are coefficients independent of ϕ_B. In view of Eq. (3.26), we will use Eq. (C.3) for $k=n+1$. Having in mind Eqs. (C.1) and (C.2), we conclude that only the highest-order Fourier mode in Eq. (C.3) will give contribution to the integral in Eq. (3.26). For this reason, the explicit form of the coefficients $a_{j,k}$ and $b_{j,k}$ (that multiply modes of lower order) is not important.

Using the method of *mathematical induction* we will prove that

$$H_k\equiv\frac{2^k}{q^k}\frac{\partial^k}{\partial \rho_B^k}\left\{K_m(q\rho_A)\cos\left[m\left(\phi_A-\phi_{A,m}\right)\right]\right\}$$
$$=\sum_{j=0}^{k-1}\left[A_{j,k}\cos(j\phi_B)+B_{j,k}\sin(j\phi_B)\right]+\frac{L^k}{\rho_A^k}\left\{K_{m+k}(q\rho_A)\cos\left[m\left(\phi_A-\phi_{A,m}\right)+k\phi_B\right]+K_{m-k}(q\rho_A)\cos\left[m\left(\phi_A-\phi_{A,m}\right)-k\phi_B\right]\right\} \quad (C.4)$$

where $A_{j,k}$ and $B_{j,k}$ are coefficients, which may depend on ρ_A, ρ_B, and ϕ_A. First we check whether Eq. (C.4) is fulfilled for $k=1$. For this goal, from Eqs. (3.1) and (3.2) we obtain the following connections between the two sets of polar coordinates:

$$\rho_A=\left(L^2+\rho_B^2-2L\rho_B\cos\phi_B\right)^{1/2},\ \phi_A=\arctan\left(\frac{\rho_B\sin\phi_B}{L-\rho_B\cos\phi_B}\right). \quad (C.5)$$

The differentiation of Eq. (C.5) yields:

$$\frac{\partial\rho_A}{\partial\rho_B}=\frac{\rho_B}{\rho_A}-\frac{L\cos\phi_B}{\rho_A},\ \frac{\partial\phi_A}{\partial\rho_B}=\frac{L\sin\phi_B}{\rho_A^2}. \quad (C.6)$$

With the help of Eq. (C.6), we obtain:

$$H_1\equiv\frac{2}{q}\frac{\partial}{\partial\rho_B}\left\{K_m(q\rho_A)\cos\left[m\left(\phi_A-\phi_{A,m}\right)\right]\right\} \quad (C.7)$$
$$=2K'_m(q\rho_A)\left(\frac{\rho_B}{\rho_A}-\frac{L\cos\phi_B}{\rho_A}\right)\cos\left[m\left(\phi_A-\phi_{A,m}\right)\right]-\frac{2m}{q\rho_A}K_m(q\rho_A)\frac{L\sin\phi_B}{\rho_A}\sin\left[m\left(\phi_A-\phi_{A,m}\right)\right].$$

Using Eq. (3.19) and the formula [68,69,80]

$$\frac{2m}{\xi}K_m(\xi)=K_{m+1}(\xi)-K_{m-1}(\xi) \quad (C.8)$$

we represent Eq. (C.7) in the form

$$H_1=2K'_m(q\rho_A)\frac{\rho_B}{\rho_A}\cos\left[m\left(\phi_A-\phi_{A,m}\right)\right] \quad (C.9)$$
$$+\left[K_{m+1}(q\rho_A)+K_{m-1}(q\rho_A)\right]\frac{L\cos\phi_B}{\rho_A}\cos\left[m\left(\phi_A-\phi_{A,m}\right)\right]-\left[K_{m+1}(q\rho_A)-K_{m-1}(q\rho_A)\right]\frac{L\sin\phi_B}{\rho_A}\sin\left[m\left(\phi_A-\phi_{A,m}\right)\right].$$

The final form of Eq. (C.9) is

$$H_1=2K'_m(q\rho_A)\frac{\rho_B}{\rho_A}\cos\left[m\left(\phi_A-\phi_{A,m}\right)\right]+\frac{L}{\rho_A}\left\{K_{m+1}(q\rho_A)\cos\left[m\left(\phi_A-\phi_{A,m}\right)+\phi_B\right]+K_{m-1}(q\rho_A)\cos\left[m\left(\phi_A-\phi_{A,m}\right)-\phi_B\right]\right\}. \quad (C.10)$$

Denoting the first term in the right-hand side of Eq. (C.10) by $A_{0,1}$, we arrive at the conclusion that Eq. (C.4) is satisfied for $k=1$.

Next, we will show that if Eq. (C.4) is valid for a given value of k, then it holds also for $k+1$. We multiply Eq. (C.4) by $2/q$ and take derivative with respect to ρ_B from the obtained result:

$$\begin{aligned} H_{k+1} \equiv & \frac{2^{k+1}}{q^{k+1}} \frac{\partial^{k+1}}{\partial \rho_B^{k+1}} \left\{ K_m(q\rho_A) \cos\left[m\left(\phi_A - \phi_{A,m}\right)\right]\right\} \\ = & \frac{2}{q}\frac{\partial}{\partial \rho_B} \sum_{j=0}^{k-1} \left[A_{j,k}\cos(j\phi_B) + B_{j,k}\sin(j\phi_B)\right] \\ & + \frac{2}{q}\frac{\partial}{\partial \rho_B}\left\{ \frac{L^k}{\rho_A^k} K_{m+k}(q\rho_A)\cos\left[m\left(\phi_A - \phi_{A,m}\right) + k\phi_B\right]\right\} \\ & + \frac{2}{q}\frac{\partial}{\partial \rho_B}\left\{ \frac{L^k}{\rho_A^k} K_{m-k}(q\rho_A)\cos\left[m\left(\phi_A - \phi_{A,m}\right) - k\phi_B\right]\right\}. \end{aligned} \quad \text{(C.11)}$$

Using Eq. (C.6), after some transformations we represent Eq. (C.1) in the form:

$$\begin{aligned} H_{k+1} = & \sum_{j=0}^{k} \left[C_{j,k}\cos(j\phi_B) + D_{j,k}\sin(j\phi_B)\right] \\ & + \left[\frac{m+k}{q\rho_A} K_{m+k}(q\rho_A) - K'_{m+k}(q\rho_A)\right] \frac{L^{k+1}}{\rho_A^{k+1}} \cos\left[m\left(\phi_A - \phi_{A,m}\right) + (k+1)\phi_B\right] \\ & - \left[\frac{m-k}{q\rho_A} K_{m-k}(q\rho_A) + K'_{m-k}(q\rho_A)\right] \frac{L^{k+1}}{\rho_A^{k+1}} \cos\left[m\left(\phi_A - \phi_{A,m}\right) - (k+1)\phi_B\right] \end{aligned} \quad \text{(C.12)}$$

where $C_{j,k}$ and $D_{j,k}$ are coefficients, which may depend on ρ_A, ρ_B, and ϕ_A. Using again Eqs. (3.19) and (C.8), we bring Eq. (C.12) in the form:

$$\begin{aligned} H_{k+1} = & \sum_{j=0}^{k} \left[C_{j,k}\cos(j\phi_B) + D_{j,k}\sin(j\phi_B)\right] \\ & + K_{m+k+1}(q\rho_A) \frac{L^{k+1}}{\rho_A^{k+1}} \cos\left[m\left(\phi_A - \phi_{A,m}\right) + (k+1)\phi_B\right] \\ & + K_{m-(k+1)}(q\rho_A) \frac{L^{k+1}}{\rho_A^{k+1}} \cos\left[m\left(\phi_A - \phi_{A,m}\right) - (k+1)\phi_B\right]. \end{aligned} \quad \text{(C.13)}$$

Eq. (C.13) is equivalent to Eq. (C.4) for $k+1$, which proves the validity of Eq. (C.4) for all $k \geq 1$.

Furthermore, in Eq. (C.4) we carry out the limiting transition $\rho_B = r_\delta \to 0$, which leads to $\rho_A \to L$ and $\phi_A \to 0$; see Eq. (C.5). In the same limit, the coefficient functions $C_{j,k}$ and $D_{j,k}$ tend to numbers that are independent of ϕ_B, which will be denoted as follows: $C_{j,k} \to a_{j,k}$, and $D_{j,k} \to b_{j,k}$. Then, the limiting form of Eq. (C.4) for $\rho_B = r_\delta \to 0$ coincides exactly with Eq. (C.3) and thus proves its validity.

In Eq. (C.3), we set $k = n+1$, substitute the result in Eq. (3.26), and use the orthogonality relations (C.1) and (C.2):

$$\begin{aligned} F_x = & -\frac{q\gamma h_{A,m} h_{B,n}}{2K_m(qr_A)K_n(qr_B)} \int_0^{2\pi} d\phi_B \\ & \times \left\{ K_{m+n+1}(qL)\cos\left[(n+1)\phi_B - m\phi_{A,m}\right]\cos\left[(n+1)\phi_B - n\phi_{B,n}\right] \right. \\ & \left. + K_{m-n-1}(qL)\cos\left[(n+1)\phi_B + m\phi_{A,m}\right]\cos\left[(n+1)\phi_B - n\phi_{B,n}\right]\right\} \end{aligned} \quad \text{(C.14)}$$

With the help of the known formula $2\cos\alpha\cos\beta = \cos(\alpha+\beta) + \cos(\alpha-\beta)$, we finally arrive at Eq. (3.27).

For calculation of the functions $G_j(x)$ in Eq. (3.29) for $j>1$, we integrate Eq. (3.19):

$$K_{j-1}(x) = \frac{1}{2}\left[\int_x^\infty K_j(\xi)d\xi + \int_x^\infty K_{j-2}(\xi)d\xi\right] \quad \text{(C.15)}$$

Using the definition in Eq. (3.30), we obtain the following recurrence formula:

$$G_j(x) = 2K_{j-1}(x) - G_{j-2}(x), \; j = 2, 3, \ldots \quad \text{(C.16)}$$

Knowing $G_0(x)$ and $G_1(x)$ from Eqs. (3.31) and (3.32), we can further calculate the values of $G_j(x)$ for $j \geq 2$. The modified Struve functions $\boldsymbol{L}_{-1}(x)$ and $\boldsymbol{L}_0(x)$ that enter Eq. (3.32), can be accurately calculated by using computational software programs like 'Mathematica', or from the series expansions [79,83]:

$$\boldsymbol{L}_0(x) = \frac{2}{\pi}\left(x + \frac{x^3}{1^2 3^2} + \frac{x^5}{1^2 3^2 5^2} + \frac{x^7}{1^2 3^2 5^2 7^2} + \ldots\right) \quad \text{(C.17)}$$

$$\boldsymbol{L}_{-1}(x) = \frac{d}{dx}\boldsymbol{L}_0(x) = \frac{2}{\pi}\left(1 + \frac{z^2}{1^2 3} + \frac{z^4}{1^2 3^2 5} + \frac{z^6}{1^2 3^2 5^2 7} + \ldots\right). \quad \text{(C.18)}$$

References

[1] Kralchevsky PA, Nagayama K. Particles at fluid interfaces and membranes. Amsterdam: Elsevier; 2001.
[2] Binks BP, Horozov TS, editors. Colloidal particles at liquid interfaces. Cambridge: Cambridge University Press; 2006.
[3] Kralchevsky PA, Denkov ND. Capillary forces and structuring in layers of colloid particles. Curr Opin Colloid Interface Sci 2001;6:383–401.
[4] Zeng C, Bissig H, Dinsmore AD. Particles on droplets: from fundamental physics to novel materials. Solid State Commun 2006;139:547–56.
[5] Hunter TN, Pugh RJ, Franks GV, Jameson GJ. The role of particles in stabilising foams and emulsions. Adv Colloid Interface Sci 2008;137:57–81.
[6] Oettel M, Dietrich S. Colloidal interactions at fluid interfaces. Langmuir 2008;24:1425–41.
[7] Kralchevsky PA, Danov KD, Denkov ND. Chemical physics of colloid systems and interfaces. In: Birdi KS, editor. Handbook of surface and colloid chemistry. third edition. Boca Raton (FL): CRC Press; 2009. p. 197–377.
[8] Kralchevsky PA, Danov KD. Interactions between particles at a fluid interface. In: Starov VM, editor. Nanoscience: colloidal and interfacial aspects. Boca Raton (FL): CRC Press; 2010. Chapter 15.
[9] Nicolson MM. The interaction between floating particles. Proc Cambridge Philos Soc 1949;45:288–95.
[10] Chan DYC, Henry JD, White LR. The interaction of colloidal particles collected at fluid interfaces. J Colloid Interface Sci 1981;79:410–8.
[11] Paunov VN, Kralchevsky PA, Denkov ND, Nagayama K. Lateral capillary forces between floating submillimeter particles. J Colloid Interface Sci 1993;157:100–12.
[12] Kralchevsky PA, Nagayama K. Capillary interactions between particles bound to interfaces, liquid films and biomembranes. Adv Colloid Interface Sci 2000;85:145–92.
[13] Vassileva ND, van den Ende D, Mugele F, Mellema J. Capillary forces between spherical particles floating at a liquid–liquid interface. Langmuir 2005;21:11190–200.
[14] Kralchevsky PA, Paunov VN, Ivanov IB, Nagayama K. Capillary meniscus interactions between colloidal particles attached to a liquid–fluid interface. J Colloid Interface Sci 1992;151:79–94.
[15] Denkov ND, Velev OD, Kralchevsky PA, Ivanov IB, Yoshimura H, Nagayama K. Mechanism of formation of two-dimensional crystals from latex particles on substrates. Langmuir 1992;8:3183–90.
[16] Kralchevsky PA, Paunov VN, Denkov ND, Ivanov IB, Nagayama K. Energetical and force approaches to the capillary interactions between particles attached to a liquid–fluid interface. J Colloid Interface Sci 1993;155:420–37.
[17] Yamaki M, Higo J, Nagayama K. Size-dependent separation of colloidal particles in two-dimensional convective self-assembly. Langmuir 1995;11:2975–8.
[18] Denkov ND, Yoshimura H, Nagayama K. Method for controlled formation of vitrified films for cryo-electron microscopy. Ultramicroscopy 1996;65:147–58.
[19] Di Leonardo R, Saglimbeni F, Ruocco G. Very-long-range nature of capillary interactions in liquid films. Phys Rev Lett 2008;100:106103.
[20] Di Leonardo R, Ianni F, Saglimbeni F, Ruocco G, Keen S, Leach J, Padgett M. Optical trapping studies of colloidal interactions in liquid films. Colloids Surf, A Physicochem Eng Asp 2009;343:133–6.
[21] Velikov KP, Durst F, Velev OD. Direct observation of the dynamics of latex particles confined inside thinning water–air films. Langmuir 1998;14:1148–55.
[22] Danov KD, Pouligny B, Kralchevsky PA. Capillary forces between colloidal particles confined in a liquid film: the finite-meniscus problem. Langmuir 2001;17:6599–609.
[23] Nikolaides MG, Bausch AR, Hsu MF, Dinsmore AD, Brenner MP, Gay C, Weitz DA. Electric-field-induced capillary attraction between like-charged particles at liquid interfaces. Nature 2002;420:299–301.
[24] Danov KD, Kralchevsky PA, Boneva MP. Electrodipping force acting on solid particles at a fluid interface. Langmuir 2004;20:6139–51.
[25] Oettel M, Domínguez A, Dietrich S. Effective capillary interaction of spherical particles at fluid interfaces. Phys Rev E 2005;71:051401.

[26] Würger A, Foret L. Capillary attraction of colloidal particles at an aqueous interface. J Phys Chem B 2005;109:16435–8.
[27] Danov KD, Kralchevsky PA. Electric forces induced by a charged colloid particle attached to the water–nonpolar fluid interface. J Colloid Interface Sci 2006;298: 213–31.
[28] Danov KD, Kralchevsky PA, Boneva MP. Shape of the capillary meniscus around an electrically charged particle at a fluid interface: comparison of theory and experiment. Langmuir 2006;22:2653–67.
[29] Leunissen ME, Zwanikken J, van Roij R, Chaikin PM, van Blaaderen A. Ion partitioning at the oil–water interface as a source of tunable electrostatic effects in emulsions with colloids. Phys Chem Chem Phys 2007;9:6405–14.
[30] Domínguez A, Oettel M, Dietrich S. Force balance of particles trapped at fluid interfaces. J Chem Phys 2008;128:114904.
[31] Lucassen J. Capillary forces between solid particles in fluid interfaces. Colloids Surf 1992;65:131–7.
[32] Stamou D, Duschl C, Johannsmann D. Long-range attraction between colloidal spheres at the air–water interface: the consequence of an irregular meniscus. Phys Rev E 2000;62:5263–72.
[33] Kralchevsky PA, Denkov ND, Danov KD. Particles with an undulated contact line at a fluid interface: interaction between capillary quadrupoles and rheology of particulate monolayers. Langmuir 2001;17:7694–705.
[34] Danov KD, Kralchevsky PA, Naydenov BN, Brenn G. Interactions between particles with an undulated contact line at a fluid interface: capillary multipoles of arbitrary order. J Colloid Interface Sci 2005;287:121–34.
[35] Horozov TS, Aveyard R, Binks BP, Clint JH. Structure and stability of silica particle monolayers at horizontal and vertical octane–water interfaces. Langmuir 2005;21:7405–12.
[36] Horozov TS, Binks BP. Particle behavior at horizontal and vertical fluid interfaces. Colloids Surf, A Physicochem Eng Asp 2005;267:64–73.
[37] Horozov TS, Binks BP, Aveyard R, Clint JH. Effect of particle hydrophobicity on the formation and collapse of fumed silica particle monolayers at the oil–water interface. Colloids Surf, A Physicochem Eng Asp 2006;282:377–86.
[38] Safouane M, Langevin D, Binks BP. Effect of particle hydrophobicity on the properties of silica particle layers at the air–water interface. Langmuir 2007;23: 11546–53.
[39] Basavaraj MG, Fuller GG, Fransaer J, Vermant J. Packing, flipping, and buckling transitions in compressed monolayers of ellipsoidal latex particles. Langmuir 2006;22:6605–12.
[40] de Graaf J, Dijkstra M, van Roij R. Triangular tessellation scheme for the adsorption free energy at the liquid–liquid interface: towards nonconvex patterned colloids. Phys Rev E 2009;80:051405.
[41] Loudet JC, Alsayed AM, Zhang J, Yodh AG. Capillary interactions between anisotropic colloidal particles. Phys Rev Lett 2005;94:018301.
[42] Loudet JC, Yodh AG, Pouligny B. Wetting and contact lines of micrometer-sized ellipsoids. Phys Rev Lett 2006;97:018304.
[43] Loudet JC, Pouligny B. Self-assembled capillary arrows. EPL-Europhys Lett 2009;85:28003.
[44] van Nierop EA, Stijnman MA, Hilgenfeldt S. Shape-induced capillary interactions of colloidal particles. EPL-Europhys Lett 2005;72:671–7.
[45] Lehle H, Noruzifar E, Oettel M. Ellipsoidal particles at fluid interfaces. Eur Phys J, E 2008;26:151–60.
[46] Lewandowski EP, Bernate JA, Searson PC, Stebe KJ. Rotation and alignment of anisotropic particles on nonplanar interfaces. Langmuir 2008;24:9302–7.
[47] Lewandowski EP, Bernate JA, Tseng A, Searson PC, Stebe KJ. Oriented assembly of anisotropic particles by capillary interactions. Soft Matter 2009;5:886–90.
[48] Bowden N, Terfort A, Carbeck J, Whitesides GM. Self-assembly of mesoscale objects into ordered two-dimensional arrays. Science 1997;276:233–5.
[49] Bowden N, Choi IS, Grzybowski BA, Whitesides GM. Mesoscale self-assembly of hexagonal plates using lateral capillary forces: synthesis using the capillary bond. J Am Chem Soc 1999;121:5373–91.
[50] Wolfe DB, Snead A, Mao C, Bowden NB, Whitesides GM. Mesoscale self-assembly: capillary interactions when positive and negative menisci have similar amplitudes. Langmuir 2003;19:2206–14.
[51] Brown ABD, Smith CG, Rennie AR. Fabricating colloidal particles with photolithography and their interactions at an air–water interface. Phys Rev E 2000;62: 951–60.
[52] Boneva MP, Christov NC, Danov KD, Kralchevsky PA. Effect of electric-field-induced capillary attraction on the motion of particles at an oil–water interface. Phys Chem Chem Phys 2007;9:6371–84.
[53] Boneva MP, Danov KD, Christov NC, Kralchevsky PA. Attraction between particles at a liquid interface due to the interplay of gravity- and electric-field-induced interfacial deformations. Langmuir 2009;25:9129–39.
[54] Fernández-Toledano JC, Moncho-Jordá A, Martínez-López F, Hidalgo-Álvarez R. Theory for interactions between particles in monolayers. In: Binks BP, Horozov TS, editors. Colloidal particles at liquid interfaces. Cambridge: Cambridge University Press; 2006. p. 108–51.
[55] Bordács S, Agod A, Hórvölgyi Z. Compression of Langmuir films composed of fine particles: collapse mechanism and wettability. Langmuir 2006;22:6944–50.
[56] Forny L, Pezron I, Saleh K, Guigon P, Komunjer L. Storing water in powder form by self-assembling hydrophobic silica nanoparticles. Powder Technol 2007;171: 15–24.
[57] Gao B, Steenhuis TS, Zevi Y, Morales VL, Nieber JL, Richards BK, McCarthy JF, Parlange J-Y. Capillary retention of colloids in unsaturated porous media. Water Resour Res 2008;44:W04504.
[58] Xu T, Jin M, Xie Z, Jiang Z, Kuang Q, Wu H, Huang R, Zheng L. Tensions at liquid interfaces: a general filter for the separation of micro-/nanoparticles. Langmuir 2008;24:2281–3.
[59] Brugger B, Rutten S, Phan KH, Moller M, Richtering W. The colloidal suprastructure of smart microgels at oil–water interfaces. Angew Chem Int Ed 2009;48:3978–81.
[60] Ma H, Dai LL. Structure of multi-component colloidal lattices at oil–water interfaces. Langmuir 2009;25:11210–5.
[61] Kurella AK, Samant AN, Dahotre NB. Laser surface multilevel self-assembly of CaP–TiO_2 particles. J Appl Phys 2009;105:014913.
[62] Acharya S, Efrima S. Two-dimensional pressure-driven nanorod-to-nanowire reactions in Langmuir monolayers at room temperature. J Am Chem Soc 2005;127: 3486–90.
[63] Fournier JB, Galatola P. Anisotropic capillary interactions and jamming of colloidal particles trapped at a liquid–fluid interface. Phys Rev E 2002;65:031601.
[64] Thareja P, Velankar S. Rheology of immiscible blends with particle-induced drop clusters. Rheol Acta 2008;47:189–200.
[65] Zhou W, Cao J, Liu W, Stoyanov S. How rigid rods self-assemble at curved surfaces. Angew Chem Int Ed 2008;47:1–5.
[66] Madivala B, Fransaer J, Vermant J. Self-assembly and rheology of ellipsoidal particles at interfaces. Langmuir 2009;25:2718–28.
[67] Madivala B, Vandebril S, Fransaer J, Vermant J. Exploiting particle shape in solid stabilized emulsions. Soft Matter 2009;5:1717–27.
[68] Janke E, Emde F, Lösch F. Tables of higher functions. New York: McGraw-Hill; 1960.
[69] Dwight HB. Tables of integrals and other mathematical data. 4th edition. New York: Macmillan Company; 1964.
[70] Robinson DJ, Earnshaw JC. Experimental study of colloidal aggregation in two dimensions. II. Kinetic aspects. Phys Rev A 1992;46:2055–64.
[71] Reynaert S, Moldenaers P, Vermant J. Control over colloidal aggregation in monolayers of latex particles at the oil–water interface. Langmuir 2006;22: 4936–45.
[72] Vassileva ND, van den Ende D, Mugele F, Mellema J. Restructuring and break-up of two-dimensional aggregates in shear flow. Langmuir 2006;22:4959–67.
[73] Pergamenshchik VM. Strong collective attraction in colloidal clusters on a liquid–air interface. Phys Rev E 2009;79:011407.
[74] Ono S, Kondo S. Molecular theory of surface tension in liquids. In: Flügge S, editor. Handbuch der Physik, vol. 10. Berlin: Springer; 1960. p. 134.
[75] Velev OD, Denkov ND, Paunov VN, Kralchevsky PA, Nagayama K. Direct measurement of lateral capillary forces. Langmuir 1993;9:3702–9.
[76] Brand L. Vector and tensor analysis. New York: Wiley; 1947.
[77] Verwey EJW, Overbeek JThG. The theory of stability of lyophobic colloids. Amsterdam: Elsevier; 1948.
[78] Kralchevsky PA, Nagayama K. Capillary forces between colloidal particles. Langmuir 1994;10:23–36.
[79] Abramowitz M, Stegun IA. Handbook of mathematical functions. New York: Dover; 1965.
[80] Korn GA, Korn TM. Mathematical handbook. New York: McGraw-Hill; 1968.
[81] Arfken GB. Mathematical methods for physicists. second edition. London: Academic Press; 1970.
[82] Struve H. Beitrag zur Theorie der Diffraction an Fernröhren. Ann Physik Chemie 1882;17:1008–16.
[83] Prudnikov AP, Marichev OI, Brychkov YuA. Integrals and series, vol. 3: more special functions. Newark, NJ: Gordon and Breach; 1990. p. 24–7.